# Comprehensive genomic analysis of *Trypanosoma rangeli* reveals key insights into the biology and evolution of this non-virulent American mammalian trypanosome

Guilherme Augusto Maia[1,2*], Gabriel Machado Matos[1,3*], Adriana Corrêa da Silva[1,4*], Caibe Alves Pereira[1], Carime Lessa Mansur Pontes[1], Debora Denardin Lückmeyer[1], Rafaela Andrade do Carmo[4], Renato Simões Moreira[5], Thaynara Karoliny de Souza Pereira[1], Amábilli de Souza Rosar[1], Theo Cardozo Brascher[6], Guilherme Razzera[6], José Franco da Silveira Filho[4], Mário Steindel[1], Patrícia Hermes Stoco[1], Glauber Wagner[1], Björn Andersson[7**], Edmundo Carlos Grisard[1**]

** Correspondence: bjorn.andersson@ki.se; edmundo.grisard@ufsc.br.

Department of Cell and Molecular Biology, Karolinska Institutet, P.O. Box 285, SE-171 77, Stockholm, Sweden. Phone: +46 852483987.

Universidade Federal de Santa Catarina, Campus Trindade. Setor F, Bloco G, Sala G809. Trindade, Florianópolis - SC, 88040-900, Brazil. Phone: +55 48 37214551.

The full list of author information is available at the end of the article

* These authors have equally contributed to this work.

**ABSTRACT**

**Background:** *Trypanosoma rangeli* is a non-virulent hemoflagellate protozoan parasite that infects mammals, including humans, in Central and South America. It is primarily transmitted through the bites of triatomine bugs and shares an overlapping geographical distribution with *T. cruzi*, as well as triatomine vectors and mammalian hosts, and various shared surface antigens. The life cycle of *T. rangeli* differs from those of other human-infecting trypanosomes, such as *T. cruzi* and *T. brucei*, and the molecular mechanisms underlying host-parasite and host-vector interactions are not well understood, demanding improved molecular and genomic resources.

**Results:** The use of a hybrid approach to sequence and assemble the *T. rangeli* genome, complemented by transcriptomics and proteomics for functional gene annotation, led to the generation of the near-complete genome sequence of the parasite. Detailed intra- and inter-specific comparative genomics allowed analysis of polymorphisms, genome structure and improved resolution of genes coding for important surface molecules such as Mucins, TASV and GP63.

**Conclusions:** The improved *T. rangeli* genome assembly, combined with comparative genomics has yielded novel biological insights. These included the first description of a metalloprotease activity, attributed to specific GP63 genes that are absent in *Leishmania* species. In addition, a TASV gene family that is absent in *T. cruzi* was identified, which indicates a possible role in the *T. rangeli* infection process.

**Keywords**: Trypanosomiasis, Avirulent trypanosome, Comparative genomics, Surface molecules.

## 1. BACKGROUND

Trypanosomatids are a group of single-celled, mono-flagellated organisms belonging to the class Kinetoplastea. This group includes etiological agents of neglected tropical diseases of humans such as *Trypanosoma cruzi* (Chagas disease or American trypanosomiasis), *Trypanosoma brucei* (African sleeping sickness), and *Leishmania* spp. (Leishmaniasis) [1]. Collectively, these neglected and socially determined tropical diseases collectively affect more than 18 million people worldwide, mostly in the developing countries [2,3].

*Trypanosoma rangeli* [4], is a mammalian parasite species found in Central and South America, primarily transmitted via bite of triatomine vectors. Unlike *T. brucei* and *T. cruzi*, *T. rangeli* is considered non-virulent to mammalian hosts, despite the genetic and antigenic similarity with *T. cruzi* and its inoculative mode of transmission [5,6]. On the other hand, *T. rangeli* is harmful to insect vectors, particularly within the genus *Rhodnius* [7–9].

Reports of natural mixed infections by *T. rangeli* and *T. cruzi* have been documented in a variety of mammalian hosts and triatomine vectors species throughout Central and South America [4,7,10–12]. However, the prevalence of human infection by *T. rangeli* remains unclear. The sympatric occurrence, along with shared hosts, vectors and several antigens, leads to the possibility of a strong serological cross-reactivity [13–15].

*T. rangeli* infection biology is understudied. Previously, comparative analyses of isolated genes coding for surface antigens or related to cell infection or evasion of the immune system, partial genomic [5,16], transcriptomic [17], and proteomic datasets [18] have been produced.

Comparative biological and molecular studies have revealed the presence of trans-sialidase, one of the most important and well-studied virulence factors of *T. cruzi*, and the surface glycoprotein 63 (GP63) metalloprotease (also known as Leishmaniolysin), this major surface protease of *Leishmania* spp. plays a crucial role in cell infection and intracellular survival of both *Leishmania* [19], and *T. cruzi* [20].

The *T. rangeli* genome has been estimated to be around 21-24 million base pairs (Mbp) [5,16] in size, sharing over 90% of the core genome with the pathogenic

trypanosomatids. However, these estimates are based on fragmented assemblies containing 3,436 (AM80) and 9,066 (SC58) scaffolds, respectively. While incomplete, these studies revealed that the *T. rangeli* genome is smaller, less repetitive and with shorter telomeric and sub-telomeric regions compared to the *T. cruzi* genome [21–23]. Additionally, it was proposed that the number of *T. rangeli* genes coding for virulence factors or proteins associated with pathogenesis varies between strains from different lineages and differs from those of *T. cruzi* [24,25]. For instance, compared to *T. cruzi*, *T. rangeli* has a similar number of genes coding for GP63, reduced numbers of genes coding for sialidases/trans-sialidases and Mucin-Associated Surface Proteins (MASP), and, interestingly, an increased number of genes coding for Kinetoplastid Membrane Protein 11 (KMP-11) [5,16].

Trypanosomatid genomes contain syntenic regions where genes are organized in directional transcription clusters, separated by strand-switch regions [5,25–28]. Gene families encoding surface proteins are mostly contained within repetitive regions [24,26,29,30]. Recent proposals suggested that regions of the *T. cruzi* genome that are rich in surface protein-coding genes are involved in generating antigenic diversity through gene recombination and conversion events due to the micro-homology of their flanking regions [23]. Additionally, it has been suggested that DNA replication origins in the *T. cruzi* genome are unevenly dispersed across the genome, as indicated by the enrichment of Orc1Cdc6, a component of the pre-replication complex [31].

Among several aspects of trypanosomatid biology and parasitism that remain to be fully understood, the survival and reproduction of *T. rangeli* within mammalian hosts are of particular interest [32]. For this purpose, the understanding of the complete structure and plasticity of the genome is essential for facilitating comparative genomics of virulent and non-virulent trypanosomatids of mammals. We here describe a far more accurate, near-complete genome sequence *of T. rangeli*, as well as a comparative study of other *T. rangeli* strains. Our findings reveal remarkable biological differences between virulent and non-virulent trypanosomatids, pointing out the *T. rangeli* genome structure, intraspecific variability and the repertoire of surface proteins, providing insights into the parasite biology and life cycle.

## 2. RESULTS

*2.1 T. rangeli genome sequencing and assembly*

Illumina sequencing of the *T. rangeli* SC58 strain provided 9,264,332 filtered reads (~4.8Gb) and PacBio sequencing provided 361,938 filtered reads (~6.9Gb), respectively, corresponding to approximately 20x and 192x coverage. The resulting assembly is here referred to as version 2 of the *T. rangeli* SC58 genome ("*T. rangeli* SC58 V.2"), and the fragmented assembly previously published by Stoco et al. (2014) as the "SC58 reference genome". A comparison of general assembly metrics for the *T. rangeli* SC58 V.2 genome and the reference genome assembly is shown in Table 1. The *T. rangeli* SC58 V.2 genome is available in Genbank (Bioproject PRJNA1380247).

**Table 1**. Comparison of general assembly metrics of the *Trypanosoma rangeli* SC58 reference and V.2 genomes and *T. cruzi* (CL Brener Esmeraldo-like and Sylvio X10/1 strains) genomes.

Footnote: * = Data retrieved from the TriTrypDB v.65. Mbp = Million base pairs. Kbp = Thousand base pairs. aa = amino acids. Scaffold N50 indicates the scaffold length where 50% of the entire assembly is contained in contigs equal to or larger than this value. Scaffold L50 is defined as the count of the smallest number of contigs whose length sum makes up half of the genome size. “Number of hypothetical CDS” represents CDS automatically annotated as “Hypothetical protein”. “ND”= Not determined.

Cross-mapping analysis using the MUMmer4 software indicated that 99.52% of the nuclear genomic content previously described in the SC58 reference genome [5] is included in the *T. rangeli* SC58 V.2 genome. Also, 97.71%, 97.25% and 97.52% of the reads from the PIT10, Choachí and R1625 *T. rangeli* strains, respectively, were mapped to the *T. rangeli* SC58 V.2 genome. Unique copies of all 130 universal single-copy orthologs of the phylum Euglenozoa were identified, distributed across 43 different scaffolds of the *T. rangeli* SC58 V.2 genome.

A high level of synteny was observed among the *T. rangeli* genomes, with few structural variants. However, when comparing the *T. rangeli* SC58 V.2 genome assembly to the assemblies of the *T. cruzi* CL Brener Esmeraldo-like and Sylvio X10/1

137 strains, significant structural diversity was found (Additional file 1: Supplementary Figure
138 S1).

139 The V.2 genome contained tRNA genes for all 20 amino acids and the canonical
140 5.8S, 18S and 28S rRNA genes (Table 1). The V.2 genome contains fewer tRNA genes
141 than the previous reference genome [5], having a significantly higher number of rRNA
142 genes compared to other trypanosomatid genomes (Table 1). Also, a total of 62 Spliced
143 Leader (SL) RNA genes (Mini-Exon) exhibiting a high level of conservancy were
144 identified (Additional file 2: Supplementary Figure S2A) in five distinct scaffolds, ranging
145 from 9 to 16 copies/scaffold (Additional file 2: Supplementary Figure S2B).

146 The search for chromosome-specific probe sequences of *T. cruzi* within the
147 scaffolds of the *T. rangeli* SC58 V.2 genome revealed unique mapping for nine out of 11
148 *T. cruzi* probes (Additional file 3: Supplementary Table S1). When comparing the
149 TcCLB.510129.20 chromosomal probe, derived from a 1.38 Kb-long surface membrane
150 protein identified as a single-copy gene in the *T. cruzi* genome, positive BLAST results
151 were obtained with sequences annotated as “surface membrane proteins” on scaffolds
152 5 and 14 of the *T. rangeli* SC58 V.2 genome. These two scaffolds are of 0.73 and 0.45
153 Mbp, respectively, and exhibited 85.38% similarity to each other. Fourteen segments of
154 the *T. cruzi* TcCLB.510129.20 sequence matched these scaffolds, displaying similarities
155 ranging from 78.36 to 93.51% with 100% coverage. However, the regions located
156 upstream and downstream of these matches were distinct, indicating that this gene is
157 present in multiple copies within the *T. rangeli* genome.

158 Probe TcCLB.511041.40 targeting a gene coding for a 1.63 Kb-long hexose
159 transporter gene in *T. cruzi* and showed sequence similarity with several transporter
160 genes distributed in 10 scaffolds in the *T. rangeli* SC58 V.2 genome. This finding
161 supports the observations from Cabrine-Santos et al. (2009) regarding the presence of
162 duplicated genes encoding hexose transporters on different *T. rangeli* chromosomes.
163 These chromosomes range in size from approximately 500 to 650 Kb, indicating the
164 presence of paralogous genes that are specifically unique to *T. rangeli*.

165 Ten out of the 81 scaffolds of *T. rangeli* SC58 V.2 genome contain canonical
166 telomeric repeats close to their extremities, possibly corresponding to chromosomal
167 ends (Additional file 4: Supplementary Table S2). In accordance with the genome

168 topology proposed by Stoco et al. (2014), subtelomeric regions adjacent to the telomeric
169 repeats were found to contain genes from multicopy families such as (Trans-)Sialidase
170 and GP63 (Fig. 2).
171 From the 9,454 CDSs identified in the *T. rangeli* SC58 V.2 genome,
172 approximately 32.93% encode for hypothetical proteins. This proportion is comparable
173 to that of *T. brucei* TREU927 (34.37%), but notably lower than for *T. cruzi*, for example,
174 the Esmeraldo-like haplotype (47.13%) and the Sylvio X10/1 strain (73.81%). The use
175 of a hybrid assembly and meticulous annotation allowed a reduction of hypothetical
176 proteins compared to previous *T. rangeli* datasets, such as AM80 (56.72%) and the
177 SC58 reference genome (67.89%). The annotation of the *T. rangeli* SC58 V.2 genome
178 was supported by transcriptomic [17] and proteomic [18] data generated by our group,
179 demonstrating evidence of transcription and expression for 96 (1.02%) of the
180 hypothetical CDSs. The distribution of all predicted and annotated CDSs in the *T.*
181 *rangeli* SC58 V.2 genome, including notable multigenic families and the 110 potential
182 pseudogenes, is illustrated in Fig. 1. Further analysis of genes associated with the RNA
183 interference machinery (RNAi) on the *T. rangeli* SC58 V.2 genome confirmed the non-
184 functionality of this pathway, as described previously [5].
185
186 **Figure 1**: Distribution of multicopy gene families in the scaffolds of the *Trypanosoma*
187 *rangeli* SC58 V.2 genome. Scaffolds were drawn in proportion to their size, indicated in
188 million base pairs (Mbp). Core genes are represented by black boxes, and the
189 hypothetical and multicopy gene families are represented by colored boxes as
190 indicated. The position of the genes above or below the line corresponds to the direction
191 of transcription, and scaffolds containing canonical telomeric repetitions are shown in
192 detail within the black square. The highlighted region represents an enlarged view (0.05
193 Mb window) of the telomeric regions of scaffolds 22, 29, and 32.
194
195 *2.2 Repetitive genome content*
196 Excepting telomeric repeats, 11.60% of the *T. rangeli* SC58 V.2 genome consists
197 of repetitive sequences, corresponding to approximately 2.8 Mbp, of which 9.22% (~2.2
198 Mbp) comprises structural repetitive elements, while roughly ~2.38% (565,000 bp)

199 includes members of multicopy gene families. Compared to the TriTryp genomes (*T.*
200 *brucei*, *T. cruzi* and *L. major*), *T. rangeli* has the least repetitive genome when
201 compared to *T. cruzi* CL Brener (37.03%) and Sylvio X10/1 (44.86%) and to *T. brucei*
202 TREU927 strain (24.73%). This difference is primarily attributed to a lower number of
203 genes from multicopy gene families, fewer structural repetitive elements and shorter
204 telomeric sequences (Fig. 2a).
205
206 **Figure 2**. Comparison of repetitive genomic content in studied trypanosomatid species,
207 discerning structural repetitions from multicopy gene families.
208
209 Footnote: bp = base pairs. (A) Representation of repetitive genomic content in studied trypanosomatid
210 species, in total number of base pairs. (B) Detailed composition of multicopy gene families in the genome
211 of studied trypanosomatid species, relative to the respective genome size of the species. (C) Detailed
212 composition of structural repetitive elements in the genome of studied trypanosomatid species, relative to
213 the respective genome size of the species. "Ref." points to the reference genome of *T. rangeli* (SC58
214 strain), obtained from TriTrypDB v65. "V.2" indicates the *T. rangeli* SC58 V.2 genome.
215
216 Comparative analysis of the diversity of multicopy gene families in
217 trypanosomatid genomes showed that the *T. brucei* VSG family is the largest,
218 comprising over 65% of the total number of nucleotides among studied multicopy
219 genes, followed by the RHS family that is also present in *T. cruzi* (Fig. 2b). VSG genes
220 have previously been described in the *T. rangeli* AM80 genome, but these genes were
221 not found in the *T. rangeli* SC58 reference genome or in the V.2 genome (Fig. 2b).
222 Among these gene families, the (Trans-)Sialidases are highly represented across
223 the studied genomes, varying from 29.37% and 36.66% of repeated genes in the *T.*
224 *cruzi* CL Brener and Sylvio X10/1 strains, to 41.96% and 42.74% in the *T. rangeli* AM80
225 and SC58 V.2 genomes, respectively (Fig. 2b). While *T. cruzi* can transfer sialic acid
226 from the host cell to its cellular membrane through a sialyltransferase (trans-sialidase)
227 activity, *T. rangeli* sialidases differ regarding the hydrolytic substrates [33] and lacks the
228 transferase activity [34,35]. We therefore referred to *T. rangeli* sialidases as "(Trans-
229 )Sialidase".

230 GP63 is the second largest multicopy gene family in the *T. rangeli* SC58 V.2
231 genome (35.47%) (Fig. 2b). Uniquely for the American trypanosomatids, *T. cruzi* and *T.*
232 *rangeli,* the DGF-1 multicopy gene family constitutes a considerable percentage of the
233 total repetitive content (Fig. 2b).
234 Interspersed repeats substantially contributed to the repetitive content in the *T.*
235 *rangeli* SC58 V.2 genome (65.10%). In total, this is lower than in *T. cruzi* Sylvio X10/1
236 (81.83%), but considerably higher when compared to simple repeats in the SC58 V.2
237 genome (21.42%) (Fig. 2c). These interspersed repeats are composed of sequences
238 that have been found to be present in all trypanosomatid genomes included in this
239 study. Among these sequences, retroelements constitute 15.89% in the *T. rangeli* SC58
240 V.2 genome, which can be compared to 44.39% in the *T. brucei* TREU927 genome
241 (Fig. 2c).
242

243 *2.3 Analysis of orthology*

244 Orthology analysis using 42,969 CDS from *L. amazonensis*, *L. infantum*, *T.*
245 *brucei*, *T. cruzi*, and the *T. rangeli* SC58 V.2 and reference genomes resulted in 9,111
246 CDS clusters and demonstrated that 96.56% of all CDSs from these species are
247 orthologous. The orthologous core for these species constituted 4,501 clusters and the
248 distribution of these clusters between species, as well as the species-specific genes
249 (single-CDS clusters), is shown in Fig. 3.
250

251 **Figure 3**. Distribution of clusters formed among the CDS of *Leishmania amazonensis*,
252 *L. infantum*, *Trypanosoma brucei*, *T. cruzi*, the reference and the *T. rangeli* SC58 V.2
253 genomes, as well as their respective singletons.
254

255 Footnote: The result of the orthology analysis among the CDS of five species of trypanosomatids is
256 represented: *L. amazonensis* in blue, *L. infantum* in red, *T. brucei* in green, *T. cruzi* in yellow, and *T.*
257 *rangeli* in brown. The numbers within the Venn diagram represent orthologous and paralogous clusters,
258 which contain the analysed CDS. The singletons are represented as circles outside the Venn diagram.
259

260 Out of the 298 singletons identified in the *T. rangeli* SC58 V.2 genome, 166
261 (55.70%) were annotated as hypothetical proteins. From this subset, only six had a

262 functional annotation through the assignment of GO terms, and one had experimental
263 evidence of expression [18]. *In silico* characterization of this gene indicates that it
264 encodes a protein of approximately 34.76 kDa that is addressed to the cell membrane
265 of the parasite. This protein was predicted to have a transferase activity (GO:0016740),
266 specifically hexapeptidase transferase (IPR:1837) due to the presence of a conserved
267 amino acid site.
268
269 *2.4 Chromosome copy number variation and somy estimation of T. rangeli strains*
270 Whole genome ploidy was estimated by the determination of the proportion of
271 alleles in heterozygous SNP positions in all scaffolds (Fig. 4a). In all four *T. rangeli*
272 strains, a peak at 50% was observed, which is expected for diploid genomes,
273 suggesting mostly disomic strains [29,36].
274 Chromosome Copy Number Variation (CCNV) in each strain was investigated by
275 combining Read Depth Coverage (RDC) and Allele Balance (AB) analyses [29,36].
276 Here, the RDC analysis was based on the ratio between the mean coverage of each
277 scaffold and the mean coverage of all scaffolds combined (Fig. 4b). Due to the repetitive
278 content of smaller scaffolds and how repetitive regions lead to erroneous somy
279 estimates [36], CCNV estimation was restricted to longer scaffolds (0.15 Mb) (i.e.
280 scaffolds 1 to 49). Despite applying the size cutoff, some scaffolds still contained too
281 few SNPs for reliable AB estimation (Additional file 5: Supplementary Figure S3).
282 Therefore, aneuploidies were only considered in scaffolds where both RDC and AB
283 results were concordant, providing a two-step confirmation. Aneuploidies, in all cases,
284 chromosome numbers >2, were observed in all strains. Our CCNV analysis combining
285 RDC and AB estimations indicated aneuploidies in scaffolds 7, 11, 12, 24, 29, 30, and
286 47 in the reference assembly *T. rangeli* SC58 V.2 (Fig. 4b, Additional file 5:
287 Supplementary Figure S3). Similarly, aneuploidies were identified in scaffolds 7, 16, 20,
288 24, 29, 30, 32, 38, 39, 42 and 47 for strain Choachí, in scaffolds 7, 26, 29, 30 and 47 for
289 strain PIT10, and in scaffolds 24, 29, 30, 39, and 47 for strain R1625 (Fig. 4b, Additional
290 file 5: Supplementary Figure S3). Interestingly, scaffolds 29, 30, and 47 were shown to
291 have additional copies in all strains (Fig. 4c). Notably, these scaffolds are enriched with
292 genes involved in immune evasion and parasite survival, including sialidases, GPI-

293 anchored surface protein biosynthesis, cAMP signaling, RNA processing, and lipid
294 metabolism (Fig. 4d, Additional file 5: Supplementary Figure S3).
295
296 **Figure 4**: *Trypanosoma rangeli* strains are essentially diploid, with aneuploidies in
297 scaffolds enriched in immune evasion genes.
298
299 Footnote: (A) Ploidy estimation based on the proportion of alleles at heterozygous SNP positions across
300 each scaffold. (B) Aneuploidy analysis using relative depth of coverage (RDC) across the 50 longest
301 scaffolds. Dark blue indicates scaffolds where the ratio of median scaffold coverage to median genome-
302 wide coverage exceeds 1.5. (C) Allelic proportions at heterozygous SNP positions for scaffolds 29, 31,
303 and 47, supporting some estimations. Blue points represent allele proportions along each scaffold; black
304 lines indicate median values within sliding windows. (D) Gene ontology (GO) enrichment analysis of
305 scaffolds exhibiting shared aneuploidy across all strains.
306
307 *2.5 T. rangeli GP63 family*
308 A total of 76 complete GP63 gene sequences and 40 pseudogenes were
309 identified in *T. rangeli* SC58 V.2, with 26 of the pseudogenes containing an internal stop
310 codon and 14 exhibiting truncations. The complete *Tr*GP63 sequences include the full-
311 length peptidase M8 domain (NCBI CDD code: cl19482) as detailed in Additional file 6
312 (Supplementary Table S3). Most of these sequences resemble the canonical metzincin
313 class zinc proteases motif 'HEXXHXXGX(~60)H', which features a conserved
314 methionine at the base of the active site, referred to as the Met-turn. This motif was first
315 described for GP63 in *Leishmania* spp. Furthermore, the sequences contain 19 cysteine
316 residues distributed throughout [37] (Additional file 7: Supplementary Figure S4).
317 *Tr*GP63 gene sequences were classified based on a phylogenetic analysis that
318 included sequences from different kinetoplastids (Fig. 5), along with two sequences
319 from each of the 11 GP63 groups of *T. cruzi* formerly described [20]. This analysis led to
320 the classification of at least 13 distinct GP63 groups in kinetoplastids, and *T. rangeli*
321 GP63 sequences were included in 11 of these groups. Interestingly, group 12 was
322 found to be exclusive to this species. *Tr*GP63 sequences do not cluster with the G0 and
323 G1, which include sequences found in most kinetoplastids, where G0 mainly includes
324 *Leishmania* spp. sequences and monoxenous invertebrate pathogens such as *Crithidia*

325 *fasciculata* and *Leptomonas pyrrhocoris,* and G1 contains some functional *Leishmania*
326 spp. sequences (represented by LmjF-10-0460) [38,39], sequences from *Bodo saltans*,
327 *Angomonas deanei* and sequences from other *Trypanosoma* species. Thus, *Tr*GP63
328 did not group with *T. cruzi* GP63-G1, which intriguingly lacks the Met-turn, and this may
329 reduce its activity. Synteny analysis with the corresponding genomic regions of *T. cruzi*
330 DM28c confirmed the absence of these genes in *T. rangeli*, as the eight upstream and
331 downstream genes are conserved. Except for GP63 group 2, members of all other
332 groups were identified in *T. rangeli* SC58 V.2 as well as in the other three *T. rangeli*
333 strains analysed (Additional file 6: Supplementary Table S3).
334 Inter-group *Tr*GP63 amino acid sequence identities are approximately 35%,
335 whereas intra-group identities exceed 58%, with G11 being the most variable
336 (Additional file 8: Supplementary Table S4). Four groups have a single representative
337 gene in *T. rangeli* (Groups 3, 5, 7, and 8), while G4 is the largest, with 26 genes.
338 Although *Tr*GP63 grouped with most of the *T. cruzi* groups [20], we did not identify
339 active site residue conservation, except in G6, indicating that groups are formed by
340 general sequence similarity. The classification correlated with the genomic distribution
341 of *Tr*GP63, including the same classification of genes in tandem. All *Tr*GP63 in scaffold
342 3 belong to group G12, while the 13 *Tr*GP63 in tandem in scaffold 13 were from G4.
343 One GP63 gene from G5, outside the tandem locus, was also identified in this scaffold.
344 Despite exhibiting a variable presence of both signal peptide and a GPI-anchor
345 signature, most *Tr*GP63 were predicted to be N-glycosylated with an average of 0.62%
346 (± 0.42) residues in the mature protein. The majority of *Tr*GP63 groups were found to be
347 addressed to the parasite cell surface, except members of Groups 2, 6, and 8 that
348 consistently lack a predicted GPI anchor, indicating that these may act extracellularly as
349 free proteins. Some members of groups 3, 4, 9, 10, 11, and 12 showed experimental
350 evidence of protein expression on the parasite surface of epimastigotes and/or
351 trypomastigotes [18], whereas members from groups 4, 9, 10, 11, and 12 were
352 potentially secreted, while members of Groups 2, 6, and 7 were exclusively found in the
353 *T. rangeli* secretome (Additional file 6: Supplementary Table S3), corroborating the
354 hypothesis that these groups have a role as secreted glycoproteins. Interestingly,
355 proteomic evidence of expression from some pseudogenes remains to be addressed.

356

357 **Figure 5.** *Trypanosoma rangeli* displays functional secreted and surface-attached GP63
358 repertoire and species-specific groups from other Kinetoplastids.

359

360 Footnote: (**A**) Orthology analysis of GP63 in the Kinetoplastea class. Maximum-likelihood tree inferred
361 from full-length GP63 amino acid sequences. The branch scale is shown as red straight and dashed
362 lines. Colored labels indicating metalloprotease inferred activity based on ligand cavity scores are shown
363 as green (≥ 0.5), yellow (<0.5 to ≥ 0.4), and red (<0.4), representing active, indeterminate and inactive,
364 respectively. Genes organized in tandem by at least three contiguous GP63-coding genes or
365 pseudogenes are indicated by a black line on top of the scaffold number. In case of signal peptide
366 prediction indicating absence in both analyses, GPI-anchor results are considered not applicable,
367 indicated as blue lines. Detailed description of sequences and values is provided in Supplementary Table
368 5. (**B**) Structural and *in silico* functional analysis of *T. rangeli* GP63, in comparison to *Tc*GP63-G1
369 (C4B63_30g122) and *Leishmania major* (PDB: 1LML) as control. 3D Model: Box highlights the region
370 corresponding to the Zinc-binding site, where structural and functional analyses were performed. The
371 colors of the structures were assigned according to their classification: green for the highly promising
372 group, yellow for the moderately promising group, and red for the less promising group according to
373 ligand cavity scores established parameters. Zinc-binding site: Amino acid residues with close interaction
374 with the zinc ion are shown in stick representation. Molecular surface: presence of the S1' pocket is
375 demonstrated by a green arrow or absence by a red blocked arrow. P2Rank analysis: Ligand-binding
376 prediction showing predicted cavity positions by different colors. Boxes demonstrate predicted binding
377 cavity probabilities. Molecular docking: Complexes of metalloproteases with the inhibitor 1,10-
378 phenanthroline. The cyan ligand represents the highest-affinity conformation obtained for control
379 structure, while the white ligands correspond to molecular docking results for other GP63. The boxes
380 present the RMSD values (Å) and ΔG (kcal/mol) of the complexes resulting from molecular docking.

381

382 Metalloprotease activity was experimentally detected in both epimastigote and
383 trypomastigote forms of *T. rangeli*, with higher activity observed at pH 5.5. The activity
384 was considerably lower in *T. rangeli* epimastigotes compared to *T. cruzi* epimastigotes
385 and *L. braziliensis* promastigotes (Additional file 9: Supplementary Figure S5). To
386 assess the metalloprotease functionality in each *Tr*GP63 group, 15 sequences were
387 chosen to generate three-dimensional models based on the available crystal structure
388 of GP63 (leishmanolysin) of *L. major* (LmjF-10-0460/PDB: 1LML) [37]. Additionally, the
389 *Tc*GP63-G1 (C4B63_30g122) was modelled for comparative purposes, since it was
390 missing in *T. rangeli*. The models showed pTM scores ranging from 0.57 to 0.90,

391 indicating a high predictive quality (Additional file 10: Supplementary Table S5). The
392 *Tr*GP63 metalloproteases showed a molecular organization similar to the control
393 structure, shown by global RMSD values between 9.11 and 24.79 Å, with lower
394 variation observed when considering only helix B, located at the catalytic site of the
395 metalloprotease. Overall, most of the *Tr*GP63 sequences displayed a conserved
396 active/Zinc-binding site motif. Certain genes showed punctual substitutions or several
397 alterations in the key residues as identified in, for example, TrSC58v2_9356 and
398 TrSC58v2_560. Among the 15 modelled structures, only TrSC58v2_9135 (G4) and
399 TrSC58v2_1328 (G12) exhibited the large active-site cleft (S1' pocket) in the surface
400 analysis (Additional file 11: Supplementary Figure S6). Between antiparallel β-sheets in
401 the N-terminal domain, as part of the active site, we identified a loop region with
402 'GXXAWA' Motif (Additional file 5: Supplementary Figure S3), that is mimetic of the S-
403 loop, a well-characterized conformation in vertebrate metalloproteases [40,41].
404 Considering that the motif conservation and S1' pocket are important for activity
405 inference, and that other parameters may also be important, the interaction potential of
406 the active sites with ligands was assessed using P2Rank [42], which indicated that
407 seven *Tr*GP63 had a ligand cavity probability above 50%, with TrSC58v2_4795 (G4)
408 and TrSC58v2_2748 (G6) showing values close to the control structure (71%, 74%, and
409 76%, respectively). These also match the experimentally validated GP63 *T. cruzi*
410 sequences (AY266316, AY266317, AY266318) [43]. These genes were classified as a
411 highly promising group (green structures in Fig. 5b, Additional file 12: Supplementary
412 Figure S6). Further six metalloproteases, including the *Tc*GP63-G1, displayed
413 intermediary values and were classified as a moderately promising group (yellow
414 structures). Finally, three metalloproteases showed values below 40% and were
415 classified as a less promising group (red structures). Molecular docking of the Zinc-
416 binding site region with the inhibitor 1,10-phenanthroline [44] was used to infer the
417 metalloprotease activity. In the *L. major* structure used as control, the selected complex
418 displayed the inhibitor oriented toward the $Zn^{2+}$ ion with a probability of 34% and an
419 affinity of -5.54 kcal/mol. The sequences classified as highly promising showed even
420 higher probability of the inhibitor being faced to the cofactor (67 to 44 %) and low RMSD
421 variations relative to the ligand position in the control structure. *Tc*GP63-G1 presented a

422 behavior similar to that of the highly promising *Tr*GP63, regarding ligand orientation
423 towards $Zn^{2+}$ ion (probability: 56% Docking Affinity: -6.03 kcal/mol), while the structures
424 classified as moderately and less promising did not. Fig. 5b, shows the parameters for
425 the *L. major* structure (control), *Tc*GP63-G1, TrSC58v2_4795 (G4), a highly probable
426 protease that was experimentally identified by two different techniques, and represents
427 the biggest *TrGP63* group, and TrSC58v2_560 (G11) which is unlikely to be an active
428 metalloprotease, despite the high level of expression shown by proteomic analysis in
429 both epimastigotes and trypomastigotes (Fig. 5).
430
431 *2.6 T. rangeli surface Mucins/TASV*
432 A comparative analysis between the previous reference genome sequence and
433 the SC58 V.2 genome revealed an increased number of genes belonging to the mucin-
434 like family in the improved genome sequence, where 15 gene copies were found [5,17].
435 A detailed search for known signatures of mucin-like genes, such as the signal peptide,
436 GPI-anchor signal, abundance of serine and threonine residues that are likely *O*-
437 glycosylated, as well as orthology with members of the *T. cruzi* mucin-like gene family
438 (*Tc*MUC) on the SC58 V.2 genome, resulted in the identification of seven genes
439 (*Tr*MUC1 - *Tr*MUC7) that are dispersed in three scaffolds of the SC58 V.2 genome
440 (Additional file 12: Supplementary Table S6). *Tr*MUC is slightly more similar to *Tc*MUC
441 type I, sharing an identity of 56.88% ± 22.87, when compared to *Tc*MUC type II (44.34%
442 ± 23.46). Interestingly, a conserved C-terminal region of 22 amino acids is present in
443 members of the *Tr*MUC family, but not in mucins from any other kinetoplastid species
444 present in the TriTryp database (Fig. 6a).
445 A gene that encodes a 33 kDa surface protein was described in the *T. rangeli*
446 proteome as a putative mucin-like [18], here we identified it as actually belonging to the
447 *T. cruzi* Trypomastigote, Alanine, Serine and Valine rich protein glycoprotein family
448 (*Tc*TASV), previously only found in *T. cruzi* [45].
449 Based on TASV canonical features that include post-translational modifications
450 (PTM) such as *N*-glycosylation, phosphorylation, and abundance of other amino acids
451 less common in mucin-like proteins, for instance, aromatic residues (phenylalanine,
452 histidine, tryptophan, tyrosine) and cysteine, the SC58 V.2 genome contains 14 TASV-

453 coding genes, and three TASV pseudogenes, dispersed in six scaffolds. Both
454 glycoprotein families are also present in the Choachí and R1625 strains, while *Tr*MUC
455 was not found in PIT10 assembly (Additional file 12: Supplementary Table S6).

456 A phylogenetic analysis using well described protein sequences of mucin-like
457 families (*Tc*MUC type I and type II), *T. cruzi* small mucin-like family (*Tc*SMUG) [46,47],
458 and *Tc*TASV, where certain members were previously annotated as *Tc*MUC [48] is
459 shown in Fig. 6a.

460

461 **Figure 6.** Overexpression of *Trypanosoma rangeli* glycoproteins homologous to
462 *Trypanosoma cruzi* mucin-like and TASV impaired mammalian infection.

463

464 Footnote: (**A**) Phylogenetic analysis of amino acid sequences of *Tr*MUC, *Tr*TASV-like in comparison to
465 *Tc*MUC I, *Tc*MUC II, *Tc*SMUG and *Tc*TASV. β-tubulin sequences of *Trypanosoma* spp. were used as an
466 outgroup. Bold branches indicate glycoproteins more expressed in *T. cruzi* mammalian forms
467 (trypomastigote or amastigote), and dashed branches show *T. cruzi* replicative forms (epimastigote or
468 amastigote). Bootstrap of 1000 replicates. PTM Percentage is shown internally in the bars considering
469 mature protein size (excluding N- and C- terminal cleavaged sequences). NA stands for 'Non-Applicable'
470 due to a lack of signal peptide. Logo of exclusive *Tr*MUC motif and representation of two hypervariable
471 regions of *Tr*TASV showing conserved aromatic residues. Logo Y-axis: observed information content (in
472 bits), top: residues alignment position; bottom: occupancy values as gap penalty show in blue. Full
473 description of all sequences and analysis is available in Additional file 12: Supplementary Table S6. (**B**)
474 Molecular mass analysis of homologous and heterologous tagged-fused glycoproteins expressed by the
475 *T. rangeli* Choachí strain. Western blot assay of 50 µg of total protein extract of epimastigotes. Parasites
476 lineages: Wild-type = non-transfected Choachí strain; *Tc*MUCI = tagged-fused 'clone B4-5'; *Tc*MUCII =
477 tagged-fused 'clone B2-10'; *Tr*MUC3 = tagged-fused *Tr*MUC3; *Tr*TASV-like1 = tagged-fused *Tr*TASV-
478 like1; FlagGPI = synthetic gene not fused to glycoprotein. Top: glycoproteins recognized by anti-FlagTag
479 monoclonal antibody (mAb). Bottom: Loading control recognized by anti-β-tubulin mAb. Molecular weight
480 marker: Bio-Rad Dual Xtra. (**C**) Infection kinetics assessed by bloodstream parasite load in BALB/c mice
481 (n= 5 animals/group). Intraperitoneal infection of $1x10^7$ *in vitro* trypomastigotes. Data are expressed as
482 means (lines) and standard error of mean (shaded regions). Statistical analysis: two-way ANOVA and
483 Post Hoc Bonferroni´s multiple comparisons test (*p≤0.05; ***p≤0.001; ****p≤0.0001). Main biological
484 differences are shown in the graph, and full statistical differences are available in Additional file 13:
485 Supplementary Figure S7.

486

487 An assessment of the biological function of *Tr*MUC and *Tr*TASV-like genes was
488 performed by overexpressing selected homologous genes and by expressing *T. cruzi*
489 type I and II mucins (*Tc*MUC I and *Tc*MUC II) in *T. rangeli,* adopting a similar strategy to
490 that proposed by Cánepa et al. (2012). The expression analysis of *Tr*MUC, *Tr*TASV-like,
491 *Tc*MUC I and *Tc*MUC II by transfected *T. rangeli* trypomastigotes and epimastigotes
492 (Choachí strain) demonstrated an expression of hyperglycosylated molecules as
493 indicated by a comparison of their molecular weight to native proteins (Fig. 6b). Variable
494 glycosylation was observed, ranging from a 5X increment in *Tc*MUC I to 2.5x increment
495 for *Tc*MUC II-expressing parasites (Additional file 12: Supplementary Table S6).
496 Interestingly, overexpression of homologous *Tr*MUC and *Tr*TASV-like resulted in
497 less glycosylated proteins (1.6x and 1.3x, respectively) (Fig. 6b). In addition,
498 overexpression of *Tr*MUC3 by Choachí strain was impaired as indicated by a very faint
499 band around 45 kDa in a Western Blot analysis (Figure 6B), despite all sequences
500 being integrated in the same genome locus under the control of the tubulin promoter
501 and being attached to the parasite surface using the same GPI-anchor sequence.
502 Expression of these glycoproteins by *T. rangeli* altered the parasitemia profile in
503 the mammalian host, as shown in comparative infection assays in BALB/c mice with
504 wild-type and transfected trypomastigotes (Fig. 6c, Additional file 13: Supplementary
505 Figure S7).
506 In contrast with *Tc*MUC I-expressing parasites that showed no difference in
507 parasitemia from wild-type and Flag-GPI expressing parasites used as controls ($p$
508 $>0.05$), *T. rangeli* expressing *Tc*MUC II were found earlier and in higher in number in the
509 bloodstream of the experimentally infected mice from the first ($p \leq 0.05$) to the 7$^{th}$ day
510 post-infection (d.p.i.) ($p<0.001$) in comparison to controls (Fig. 6c). Overexpression of
511 *Tr*MUC and *Tr*TASV-like1 genes in *T. rangeli*, resulted in a moderate decrease in the
512 parasitemia of *Tr*TASV-like1 transfected parasites in mice between 2 ($p<0.01$) and 4
513 d.p.i. ($p \leq 0.05$) when compared to the controls. In contrast, overexpression of *Tr*MUC3
514 by *T. rangeli* was unsuccessful, as shown in Fig. 6b. Mice infected with *Tr*MUC3-
515 transfected parasites showed variable parasitemia between infected animals, and a
516 significantly reduced parasitemia between the 2$^{nd}$ and 4$^{th}$ d.p.i. ($p<0.0001$), to the 8$^{th}$
517 d.p.i. ($p<0.01$) (Fig. 6c, Additional file 13: Supplementary Figure S7). The overall

518 parasitemia in mice observed between *T. rangeli* strains from distinct genetic lineages
519 (10-12 days) was not altered by the expression of any of the studied glycoproteins.
520
521 **3. DISCUSSION**
522 The use of a hybrid deep-sequencing approach (PacBio and Illumina) for a *de*
523 *novo* assembly of the *T. rangeli* genome resulted in a more contiguous and improved
524 resolved genome sequence, especially for repetitive and complex regions containing
525 multicopy gene families and telomeric sequences. Although a large proportion of the
526 gene content was identified in the previous reference genome [5], a reduction of over
527 90% of the number of scaffolds was achieved. The use of PacBio long reads has
528 improved the contiguity of some of the complex *T. cruzi* strain genomes by resolving
529 repetitive regions [49]. Among these, strains as Bug2148 [50]; Dm28c and TCC [26];
530 Brazil and Y [51], and Sylvio X10/1 [23] have achieved a near-complete chromosomal
531 resolution. The additional use of Illumina reads in the present study have further
532 increased the contiguity and the quality of the resulting genome assembly, as well as
533 allowing intraspecific comparative analysis.
534 The identification of 10 possible telomeric regions represents a significant
535 improvement compared to the three telomeric regions previously described in the *T.*
536 *rangeli* SC58 reference genome, since sub-telomeric regions are key sites for the
537 expression of multicopy genes in trypanosomatids. Telomeric regions were not
538 identified at both ends of any of the scaffolds in the *T. rangeli* SC58 V.2 genome. In *T.*
539 *brucei*, the sub-telomeric region is responsible for the expression of VSG [52,53]. In *T.*
540 *cruzi*, the regions adjacent to the telomeres contain (Trans-)Sialidases genes, mostly
541 type II (GP82, GP90, GP85, TSA-1, SA85, and ASP-2) [54], DGF-1, and RHS [52]. In *T.*
542 *rangeli*, we have previously shown that the sub-telomeric region is shorter than that of
543 *T. cruzi*, due to the absence of multicopy genes from the (Trans-)Sialidases, DGF-1,
544 and other gene families [5].
545 Polycistronic transcription of trypanosomatids via RNA polymerase II leads to a
546 pre-mRNA that requires maturation by addition of a 39bp-long spliced leader (SL)
547 sequence at their 5' ends, providing the SL RNA splice donor site and essential motifs
548 for RNA stability and splicing recognition [55,56]. Despite such relevance, the genomic

549 organization and the sequence of SL genes in trypanosomatids vary between species.
550 The sequences of SL genes in *T. cruzi* are conserved but these genes differ widely in
551 copy number and chromosomal location between strains, often appearing on multiple
552 chromosomes [20,22,23]. In *T. brucei*, SL genes are also conserved, but far less
553 dispersed across the genome [57]. Although having a similar structure formed by an
554 exon and an intron of specific lengths as described for *T. cruzi* and *T. brucei*, the *T.*
555 *rangeli* SL genes are distinctively interspersed with the 5S rRNA genes, a feature
556 conserved among strains of distinct origins [6]. A total of 62 SL gene copies were found
557 across five distinct scaffolds on the *T. rangeli* SC58 V.2 genome, all of them exhibiting
558 the exon/intron structure and being interspersed with the 5S rRNA genes as formerly
559 described.

560 The improved resolution of this *T. rangeli* genome sequence has revealed
561 additional repetitive genomic content, but the *T. rangeli* SC58 V.2 genome still contains
562 a lower number of genes from multicopy gene families and fewer repetitive genomic
563 elements compared to *T. cruzi* and *T. brucei* overall.

564 In all studied *T. rangeli* strains, the Sialidase and GP63 families have the highest
565 numbers of genes [5,16]. The large amount of genes coding for sialidases in the *T.*
566 *rangeli* genome might be related to the involvement of this molecule during cell
567 adhesion and invasion processes as described to other trypanosomatids. Thus, it was
568 initially hypothesized that these enzymes would only be in their active states in
569 epimastigote forms in the vector insect [58]. However, it has been shown through
570 experiments using liquid chromatography coupled with mass spectrometry that
571 sialidases are the most abundant proteins identified in both the epimastigote and
572 trypomastigote forms of *T. rangeli* [18]

573 The description of VSG-coding genes in the *T. rangeli* AM80 genome by
574 Bradwell et al. (2018) was unexpected, since these surface glycoproteins have only
575 been exclusively described in African trypanosomes, such as *T. brucei*, *T. congolense*
576 and *T. vivax*, but not in *T. cruzi* or *T. rangeli* [5,22,59]. No VSG-related genes were
577 found in the assemblies or reads from all sequenced strains in this study (SC58,
578 Choachí, PIT10 and R1625), nor on previous genomic, transcriptomic or proteomic
579 studies of *T. rangeli* strains.

580 The results also show that DGF-1 is present in multiple copies in the genome of
581 all studied species of American trypanosomatids. There is experimental evidence that *T.*
582 *cruzi* trypomastigotes express DGF-1 proteins on the cell surface [60], as computational
583 predictions suggesting an integrin-like activity [60,61]. It has been suggested that DGF-
584 1 may play a role in the contaminative transmission of *T. cruzi* and other American
585 trypanosomatids [61].

586 All analysed species contain a significant portion of interspersed repeats and a
587 smaller portion of simple repeats. The number of interspersed repeats identified here
588 may be inflated due to the number of unclassified repeats present in the database used
589 [62]. The reliably classified interspersed repeats in the *T. rangeli* SC58 V.2 genome are
590 mostly Long Terminal Repeats (LTR) and Long Interspersed Nuclear Elements (LINEs).
591 The large number of unclassified sequences shows the need for further investigation of
592 the repetitive sequences in trypanosomatids to address their possible biological
593 functions.

594 Simple repeats were previously presumed to be “junk DNA”, but it is now known
595 that these repetitive elements may function as facilitators of evolution, by providing
596 gene-associated sites of genetic variation with minimal genetic load [63]. Indeed, in the
597 latest version of the genome of the Sylvio X10/1 strain of *T. cruzi*, it was shown that
598 simple repeat regions often flank multicopy genes that encode surface proteins [23].
599 This configuration could allow micro-homology processes to facilitate recombination
600 between repetitive and similar sequences, resulting in new variants of surface
601 molecules, as described in other parasites [23,64,65]. Thus, the resolution and
602 identification of these regions in the *T. rangeli* SC58 V.2 genome allows recombination
603 sites containing virulence factors to be studied in a non-pathogenic trypanosomatid
604 model.

605 The orthology analysis showed a shared core genome in all studied
606 trypanosomatids, which is represented by a cluster of 4,501 orthologous CDS groups.
607 This result is consistent with previous studies indicating that trypanosomatid organisms
608 share a significant portion of their genetic content [29,66]. In comparison, 403
609 orthologous clusters were exclusively shared between *T. cruzi* and *T. rangeli* in the
610 previous genome study of the SC58 strain, whereas this study identified 453 such

611 orthologous groups. This is not surprising, given the close phylogenetic relationship
612 between these parasites [67]. Of the set of 298 unique genes identified in the *T. rangeli*
613 SC58 V.2 genome, 166 (55.70%) are annotated as hypothetical proteins. From this
614 subset of, only one has a functional annotation by assignment of GO terms, and
615 experimental evidence of expression from MS/MS data. The *in silico* characterization of
616 this gene indicates that the corresponding protein is located in the plasma membrane of
617 the parasite, with a conserved site with hexapeptide transferase activity and a unique
618 associated peptide. The identification of this CDS is important for studies of genetic
619 markers with biotechnological applications, especially for the differential diagnosis of
620 Chagas disease.

621 It is noteworthy to mention that sequences revealing relevant but partial
622 similarities were annotated as pseudogenes on *T. rangeli* SC58 V.2 genome. These
623 may represent remnants of formerly functional genes that underwent pseudogenization
624 via a number of biological mechanisms, as proposed for *L. major*, *T. brucei*, and *T. cruzi*
625 [20,68].

626 While aneuploidies have been widely reported in trypanosomatids, including *T.*
627 *cruzi* [36,69,70] and *Leishmania* spp. [71–73], their occurrence in *T. rangeli* remains
628 underexplored. Previous studies using pulsed-field gel electrophoresis (PFGE)
629 documented chromosomal size polymorphisms across *T. rangeli* strains [5,74,75], but
630 ploidy and CCNV analyses were not performed. By using our new reference assembly,
631 with improved resolution of repetitive and complex regions, we estimated the somy of *T.*
632 *rangeli* SC58 and three additional strains (Choachí, PIT10, and R1625). The CCNV
633 analyses indicated that these genomes are mostly diploid, with aneuploidies that are
634 shared among all strains and ones that are unique to individual strains.

635 Since some trypanosomatids lack a functional RNA interference pathway [76]
636 and rely on polycistronic transcription, which limits promoter-driven regulation of
637 individual genes, chromosomal duplications can directly influence gene expression by
638 providing additional transcriptional templates [77]. The aneuploidies shared among *T.*
639 *rangeli* strains in this study were associated with scaffolds enriched with genes involved
640 in immune evasion and parasite survival, including sialidases, GPI-anchored surface
641 protein biosynthesis, cAMP signaling, RNA processing, and lipid metabolism. These

642 functions are likely essential mechanisms to evade both host and vector immune
643 responses. At the same time, the presence of aneuploidies restricted to specific
644 chromosomes in individual strains may reflect selective pressures linked to their
645 geographic distribution and the distinct host- or vector-related environments.

646 The GP63 gene copy number varies greatly among kinetoplastids. *L. major*
647 carries in total six GP63 genes, four of them arranged in tandem (Chr. 10) [78], while *L.*
648 *braziliensis* has 39 copies [79]. *T. brucei* contains about 12 genes of the orthologous
649 Major Surface Protease (MSP) divided into three families (seven MSP-A genes, four
650 MSP-B in tandem, and a single MSP-C gene) [80,81]. In contrast, *T. cruzi* (DM28c
651 strain) has 96 genes and 282 pseudogenes belonging to 11 groups [20]. We found that
652 *T. rangeli* possesses an intermediary number of 76 genes and 40 pseudogenes, in 12
653 groups, in which G12 is a species-specific group, including four groups that are likely to
654 be catalytically active and experimentally found to be secreted and/or attached to the
655 parasite surface. The G2 genes were not identified in previous studies. Neither the
656 phylogenetic nor the synteny analysis in SC58.V2 support the presence of G1 in *T.*
657 *rangeli*. Additionally, no *T. rangeli* sequence was identified as belonging to G0, the
658 group that includes the majority of *Leishmania* spp. GP63 genes, suggesting a
659 divergence in function and activity.

660 The structural and functional computational analysis of *Tr*GP63 is consistent with
661 the metalloprotease enzyme class, particularly when compared with leishmanolysin and
662 *Tc*GP63-G1. We verified the ability of these proteins to coordinate a $Zn^{2+}$ ion, an
663 essential requirement for catalytic activity [41]. The presence of the S1' pocket was only
664 identified in a few *Tr*GP63 sequences. This pocket is located near the active site and
665 has been extensively studied for its ability to accommodate inhibitory molecules and is
666 also essential for the recognition of hydrophobic amino acids present in oligopeptides
667 [40,82]. However, the absence of the active-site cleft cannot be interpreted as evidence
668 of inactivity, as its formation may depend on dynamic structural rearrangements not
669 explored in this study. Moreover, the absence of the S1' pocket may indicate that these
670 metalloproteases interact with distinct sets of ligands that do not rely on this region for
671 recognition or binding. We identified several *Tr*GP63 structures with high functional
672 potential to act as metalloproteases. This included structures with elevated ligand cavity

673 probability values as predicted by P2Rank. Additionally, the set of structures classified
674 as highly promising showed interaction modes with the inhibitor oriented toward the zinc
675 ion, which is the expected interaction pattern for this inhibitor with metalloproteases [44].
676 These findings indicate that the active sites of *Tr*GP63 display a biochemical
677 environment comparable to *L. major,* suggesting enzymatic functionality. Notably, the *T.*
678 *rangeli* metalloproteases in the highly promising group exhibited stronger functional
679 indicators than those observed for the *Tc*GP63-G4 and G6, which have already been
680 characterized as functionally active. Therefore, *Tr*GP63 may perform equivalent
681 functions and represent suitable candidates for functional substitution to verify them *in*
682 *vitro* using the *T. cruzi* CL Brener strain [43].

683 The metalloprotease activity of GP63 plays various roles across kinetoplastids,
684 including supporting parasite survival and adaptation to different hosts [43], as well as
685 contributing to basic parasite biology, such as lifecycle progression in *T. brucei* through
686 VSG release along with GPI-specific phospholipase C (GPI-PLC) [81]. In *Leishmania*
687 spp.*,* GP63 is known to act in adhesion, invasion, and immune evasion by interacting
688 with host receptors, modulating complement, degrading signaling pathways to impair
689 immune signaling and vesicular trafficking (phagolysosome biogenesis) and protecting
690 the parasite against oxidative stress [83], via lipid raft–mediated entry, collectively
691 enabling parasite survival inside macrophages [84]. Recently, this has been more
692 clearly defined by identifying the host-target substrates for GP63 [38]. There is a
693 possibility of a non-catalytic role of GP63, including the expression of inactive proteins
694 as adhesins that adhere to the fibronectin-receptor [85]. In addition, GP63 proteins are
695 also expressed by species that do not infect mammals such as *Phytomonas* spp., or
696 even in monoxenic species that develop exclusively in insects such as *Leptomonas*
697 spp., *Herpetomonas* spp., *Angomonas* spp., and *Crithidia* spp. [86]. This suggests a
698 role of GP63 in the defense against the immune system of the invertebrate host, since
699 this metalloprotease is also capable of hydrolyzing antimicrobial peptides produced by
700 insects [86]. Thus, GP63 performs several different roles, which may explain the
701 occurrence of different groups within the same species. The functions of *T. rangeli*
702 GP63 are still largely unknown. A comparative view could suggest a role in macrophage

703 survival since it is known that amastigote-like forms remain viable after internalization by
704 promonocytes [87].

705 It is known that *T. rangeli* encodes sialidases with hydrolytic activity but lacks
706 enzymes with sialic acid transglycosylase activity [88]. Thus, the finding of a GPI-
707 anchored, mucin-like protein of 33 kDa expressed by *T. rangeli* trypomastigotes [18] led
708 us to investigate the biological function of *T. rangeli* mucins as receptors of sialic acid
709 transferred from the host cell glycoconjugates to the *T. cruzi* surface [89].

710 In the *T. rangeli* SC58 V.2 genome, it has been possible to determine that this
711 protein belongs to a previously undetected glycoprotein family in *T. rangeli*: *Tr*TASV-
712 like, consisting of 13 complete genes and three pseudogenes. TASV has previously
713 only been described in *T. cruzi* [48,90]. The *Tc*TASV family is conserved among *T.*
714 *cruzi* strains with around 40 genes in three subgroups (A, B, and C) [45,48,91].
715 *Tc*TASV-C is the most studied subgroup of this family due to immunoreactivity in natural
716 and experimental infections [45,91,92]. The proteins are mainly shed through
717 extracellular vesicles by bloodstream trypomastigotes, but also attached to the parasite
718 cell [45,93]. Trypomastigotes express *Tc*TASV-C as 60 kDa glycoproteins and, to a
719 lesser degree, as 45 kDa proteins by amastigotes and epimastigotes, while the
720 theoretical molecular mass corresponds to ~36 kDa. Phosphorylation and glycosylation
721 of *Tc*TASV-C has been experimentally confirmed [91]. The difference in molecular mass
722 in *T. cruzi* trypomastigotes similar to that exhibited by the Choachí strain overexpressing
723 *Tr*TASV-like1, which strongly indicates that *Tr*TASV-like has the same PTMs as
724 *Tc*TASV.

725 It was possible to show that the overexpression of *Tr*TASV-like1 during *T. rangeli*
726 infection in mice causes a slight decrease in parasitemia at the beginning of the
727 infection. In *T. cruz*i, even more virulent strains exhibit high levels of *Tc*TASV. *Tc*TASV-
728 C delays and decreases parasitemia peaks in the acute mice model [45]. Therefore,
729 new data obtained in *T. rangeli* indicate a possible mechanism of control of parasite
730 number in the bloodstream, possibly through stimulus of phagocytosis and subsequent
731 antigen presentation, which does not necessarily lead to parasite elimination but to
732 intracellular survival instead of exposure in the bloodstream.

733 In the present genome assembly, a more accurate estimation on the copy
734 number variation of multicopy genes was achieved. We showed that *T. rangeli* has only
735 seven genes that encode mucin-like glycoproteins (*Tr*MUC), which is very different from
736 the high copy number in *T. cruzi* (e.g., 700 in the Brazil A4 strain and 797 in Y strain)
737 [51]. A very tight expression control of *the Tr*MUC3 gene product was also observed,
738 even under the control of a vector that enforces their expression (pROCK plasmid).
739 Despite the low expression level, the infection was impacted by the overexpression of
740 *Tr*MUC3 in trypomastigotes, decreasing the parasitemia in BALB/c mice. The
741 expression of *Tr*MUC thus causes the opposite effect compared to *Tc*MUC II in *T.*
742 *rangeli*, apparently decreasing the presence of parasites in the bloodstream, while
743 TcMUC II causes an increase. While the expression of *Tc*MUC I by the Choachí strain
744 does not affect the number of parasites in the blood, it is not possible to conclude that
745 there is no influence on the parasite load since this glycoprotein is preferentially
746 expressed in *T. cruzi* amastigotes [94,95], a parasite form that is still unexplored in *T.*
747 *rangeli* during mammalian infection [87], along with the incomplete understanding of the
748 tissue tropism of this avirulent trypanosomatid in mice models [32,96]. Moreover, *T.*
749 *cruzi* amastigotes do not express *Tc*TS group I (with trans-sialidase activity) [54,97],
750 alike is well-known for *T. rangeli* [98,99]. Therefore, the best conditions to express
751 *Tr*MUC might be found during an alleged amastigote phase, playing a role with
752 sialidases in an uncharted way, even in the *T. cruzi,* where these enzymes/substrates
753 are abundant. Further studies, mainly focused on characterizing the *T. rangeli*
754 glycoproteins, are needed to comprehend which glycoproteins and how this parasite
755 can acquire sialic acid from the media. Taking together the low copy number, the tight
756 expression control, and the absence of detection of any peak in the proteome studies so
757 far, we also hypothesize that *Tr*MUC is a gene family in the suppression process,
758 possibly a trace of the evolutionary speciation event.
759
760 **4. CONCLUSIONS**
761 The complexity of the trypanosomatid genomes correlates with their intricate
762 biology, presenting intra and interspecific variability mostly due to regions of highly
763 repetitive content such as sub-telomeric sequences. The combination of PacBio and

764 Illumina reads allowed for an improved version of the *T. rangeli* genome, and was also
765 useful for resolving complex and repetitive regions in the genome of the parasite, which
766 is the smallest and least repetitive among the mammalian infective trypanosomatids.
767 Among these repetitive regions, the results presented here demonstrate that the portion
768 of structural repetitive elements is large compared to the quantity of multicopy genes,
769 which is different from other trypanosomatid genomes studied. We highlight the
770 complexity of the *T. rangeli* multigene families of mucins-TASV and GP63 and their
771 involvement in the biology of the parasite.
772
773 **5. METHODS**
774 *5.1 Parasite culture, DNA extraction and sequencing*
775 Epimastigotes of *T. rangeli* strains Choachí, PIT10, R1625, and SC58 [100]
776 (Additional file 14: Supplementary Table S7) were cultured at 27ºC in liver infusion
777 tryptose (LIT) medium supplemented with 10% fetal calf serum (FCS), as described
778 previously [5]. Total DNA was extracted from exponential growth phase epimastigotes
779 using the ReliaPrep™ gDNA Tissue Miniprep System Kit (Promega). Library generation
780 and sequencing were performed at the National Genomics Infrastructure (NGI) hosted
781 by the Science for Life Laboratory, Stockholm (Sweden). *T. rangeli* DNA from all strains
782 was used to prepare paired-end libraries for Illumina (MiSeq or HiSeq 2500)
783 sequencing. Additionally, a SMRT library for PacBio (RSII) sequencing was prepared
784 only for the SC58 strain. Library preparation and DNA sequencing were carried out
785 according to the respective manufacturer's protocol.
786 *T. rangeli* Illumina reads with Q-score mean quality <30 were removed from the
787 analysis, following removal of the adapters from the high-quality reads using the
788 Trimmomatic v.0.39 software [101]. PacBio reads were trimmed based on sequence
789 length (>1Kb) using the FiltLong v.0.2.1 software (https://github.com/rrwick/Filtlong).
790
791 *5.2 Hybrid assembling of T. rangeli SC58 strain genome*
792 Hybrid assembly of the SC58 strain genome was performed *de novo* using high
793 quality PacBio reads by the software CANU v.2.2 [102], following incorporation of
794 Illumina reads into the assembly during the scaffolding and gap-filling steps, using the

795 SSPACE Standard v.3.0 [103] and GapFiller v.1-10 software [104], respectively. Both
796 steps were run through multiple iterations to compensate for base calling errors of
797 PacBio reads. Polishing of the assembled genome was performed using Illumina reads
798 with Q-score mean quality >34 using the Pilon v.1.23 software [105]. Finally, automated
799 allelic content reassignment was performed by the Purge Haplotigs software v.1.1.2
800 [106].

801 General assembly metrics of *T. rangeli* SC58 V.2 were evaluated using the
802 QUAST v.5.0.2 software [107] and mapping with the SC58 reference genome was
803 performed using the "dnadiff" algorithm of the MUMmer4 v.1.4 software [108].

804 The sequences corresponding to *T. rangeli* kDNA maxicircles and minicircles
805 were removed prior assembling using the BLASTn and BLASTx algorithms from the
806 BLAST+ software v.2.9.0 [109], against a database of kDNA sequences from *T. brucei*,
807 *T. cruzi*, and *T. rangeli*.

808 Further validation of the *T. rangeli* SC58 V.2 genome assembly was conducted
809 by mapping 130 universal single-copy orthologs of the Euglenozoa phylum using
810 BUSCO v.5.5.0 software [110], along with *in silico* mapping of *T. cruzi* probe sequences
811 specific to chromosomes 4, 37 and 39 [111] onto the SC58 V.2 genome assembly
812 (Additional file 3: Supplementary Table S1). For this later, a high-stringency (E-value
813 >1e-10, coverage >60%, identity >60%) similarity analysis of the *T. cruzi* probes against
814 the *T. rangeli* SC58 V.2 genome scaffolds were carried out using the BLASTn and
815 tBLASTx algorithms.

816

817 *5.3 Structural and functional annotation of the T. rangeli SC58 V.2 genome*

818 CDS prediction and automatic annotation were performed using the
819 AnnotaPipeline v1.0 software [112], using default parameters for similarity analysis (E-
820 value cutoff = 1e-5) and peptide identification (Q-value cut-off = 0.05). Gene prediction
821 was performed using AUGUSTUS v.3.3.3 [113] and an in-house training set composed
822 of *T. rangeli* SC58 expressed sequence tags (EST) [17] and deduced amino acid
823 sequences from the reference genome [5]. Automated annotation of CDS was based on
824 sequence similarity analysis using the BLASTp algorithm, matching with the protein
825 sequence dataset from the Swiss-Prot v.2022 [114] and TriTrypDB v.65 [115]

826 databases. CDS showing no similarity were automatically annotated as hypothetical.
827 Search for protein domains and families was performed using InterProScan v.5.61-93.0
828 [116] allowing assignment of Gene Ontology (GO) classification based on the identified
829 protein domains. Transcriptomic [17] and proteomic [18] datasets generated from
830 epimastigotes and trypomastigotes forms of *T. rangeli* were used to assess evidence of
831 gene transcription by Kallisto v.0.48.0 [117], and evidence of expression by Comet
832 v.2021.01 [118] and Percolator v.3.05.0 [119]. A profile for each protein composing the
833 final set of predicted and annotated CDS was generated using FastProtein v.1.0 [120].
834 Furthermore, CDS separated by less than 100 base pairs, along with adjacent ones
835 sharing similar annotations from the previous analysis, were manually reviewed to
836 assess the potential presence of pseudogenes.
837 Prediction of ribosomal RNA (rRNA) and transfer RNA (tRNA) was based on
838 sequence similarity (Identity >90%) with the Rfam database v.14.2 [121] using the
839 software Infernal v.1.1.2 [122] and validated based on coverage and identity via
840 BLASTn using the RNAcentral database v.20 [123].
841 Analysis of structural repetitive elements was performed using the software
842 RepeatMasker v.4.1.5 [124], disregarding insertions of bacterial origin and using a
843 custom library containing sequences specific to trypanosomatids retrieved from
844 msRepDB [62].
845 The presence of telomeric regions on the extremities (~10Kbp) of each scaffold
846 of the *T. rangeli* SC58 V.2 genome was assessed by search of the canonical telomeric
847 repeat of eukaryotes (TTAGGG)n [1,52], using the Seqtk v.1.4
848 (https://github.com/lh3/seqtk) and the Tidk v.0.2.31 software [125].
849
850 *5.4 Multicopy gene families*
851 Comparative analysis of multicopy gene families (amastins, DGF-1, GP63, KMP-
852 11, mucins, MASP, RHS, sialidase/trans-sialidases, tuzins, and Variant Surface
853 Glycoproteins - VSG) was carried out between the *T. rangeli* (SC58 V.2, SC58
854 reference genome, AM80), *T. cruzi* (CL Brener Esmeraldo-like and Sylvio X10/1), and
855 *T. brucei* (TREU927) genome.

856 Initially, a search for keywords across CDS annotations of each species genome
857 was performed using the software SeqKit v2.5.1 [126] using the following definitions as
858 queries: *amastin*, *dgf*, *dispersed, dispersed gene family*, *gp63*, *leishmanolysin*, *kmp*,
859 *kinetoplastid*, *kinetoplastid membrane protein*, *masp*, *mucin-associated*, *mucin-*
860 *associated surface protein*, *muc*, *mucin*, *rhs*, *retrotransposon*, *retrotransposon hot spot*,
861 *sialidase*, *vsg*, *surface glycoprotein*, *variant surface glycoprotein*, and *tuzin*. Related
862 terms, such as “MASP” and “Mucin-Associated Surface Proteins”, for example, were
863 considered as belonging to the same multicopy gene family to avoid redundancy. The
864 annotation of each CDS was manually curated to remove false positives and to assign
865 correct description of their products. In this sense, all genes whose automatic
866 annotation were “trans-sialidase” or “leishmaniolysin” were corrected to “sialidase”,
867 since *T. rangeli* lacks trans-sialidase activity [34], and to “GP63”, since members of this
868 multicopy gene family differs from *Leishmania* species, respectively.
869 Furthermore, a similarity analysis was then carried out between the predicted
870 CDS of each multicopy gene family and the corresponding transcript data of
871 trypanosomatid species on TriTrypDB. This step was performed by the BLASTx
872 algorithm of the software BLAST+ v.2.14.1 [109], considering an E-value cutoff of 1e-5.
873 Results from this analysis were only considered if the corresponding match presented a
874 coverage of over 30%, at least 50% identity and 50% positivity. Hence, redundancy was
875 removed once more, to ensure no sequence duplicates between the dataset obtained
876 from the similarity analysis and the recovered annotated CDS. Finally, the total number
877 of nucleotides for each multicopy gene family was obtained using the “stats" algorithm
878 of the software SeqKit.
879
880 *5.4.1 T. rangeli GP63*
881 Sequences identified by BLAST as GP63 underwent further examination using
882 the NCBI's Conserved Domain Database (CDD v3.21). Sequences shorter than 200
883 amino acids and classified as “incomplete”, “frameshift” or “interrupted Peptidase M8
884 Superfamily (cl19482)” were considered pseudogenes. Fragmented CDS with CDD e-
885 value > $1x10^{-32}$ for the Peptidase M8 Superfamily were artificially combined with
886 upstream or downstream coding sequences that contain complementary domains in the

887 most repetitive nucleotides at the break points, primarily occurring in glycine or proline
888 residues. The identification of the zinc-binding and active site was accomplished by
889 recognizing the "ZnMc astacin-like" domain (cd04280) and conducting a manual search
890 using Jalview version 2.11.4.1 [127]. The characterization of the signal peptide,
891 glycosylphosphatidylinositol (GPI) anchoring, and N-glycosylation was performed
892 through the use of SignalP v.6.0 [128], DeepTMHMM v.1.0 [129], NetGPI v.1.1 [130],
893 NetN-Glyc v.1.0 predictors, respectively.

894 Analysis of orthology of GP63 genes among trypanosomatids used a dataset of
895 156 sequences from *T. cruzi* strains Dm28c (21) [20] and CL Brener (5) [43] , *L.*
896 *infantum* JPCM5 strain (7), *L. major* Friedlin strain (6) [38,131,132], *T. brucei* TREU927
897 strain (17) [78]. In addition, sequences from *Angomonas deanei* strain Carvalho ATCC
898 PRA-265 (5), *Leptomonas pyrrhocoris* strain H10 (5), *Crithidia fasciculata* - strain Cf-CI
899 (5), and the free-living kinetoplastid *Bodo saltans* strain Lake Konstanz (8) were
900 obtained by BLASTp search in TriTrypDB using the *L. infantum* GP63 entries
901 (LinJ.10.0500 and LinJ.10.0520) as query [78,79]. Phylogenetic analysis was carried
902 out using the workflow provided by NGPhylogeny.fr [133] with default parameters of
903 each included tool. Data was then integrated using the Interactive Tree of Life (iTOL)
904 v.7.2 online tool [134]. Identity matrix analysis was performed using Clustal Omega
905 (EMBL-EBI Job Dispatcher [135]) and SIAS tool
906 (http://imed.med.ucm.es/Tools/sias.html). Active site motif was describe using
907 ScanProsite tool [136].

908 Metalloprotease activity assays were carried out using a total of $1 \times 10^8$
909 parasites, which included *Leishmania braziliensis* (MHOM/BR/75/M2904 strain
910 promastigotes), *T. cruzi* (Y strain epimastigotes), and *T. rangeli* (Choachí strain
911 epimastigotes and trypomastigotes). The parasites were lysed in a buffer containing 1%
912 Triton X-100 and 10 mM Tris-HCl at pH 6.8. SDS-PAGE gels were prepared with 0.2%
913 gelatin, and the samples were neither heated nor reduced prior to analysis. Following
914 electrophoresis, the gels were washed twice with a 0.1 M sodium acetate buffer (pH
915 5.5) that contained 2.5% Triton X-100. Subsequently, the gels were incubated for 48
916 hours at 37 °C in a buffer consisting of 0.1M sodium acetate and 1mM DTT at pH 5.5. In
917 some cases, 10mM 1,10-phenanthroline (Sigma-Aldrich) was included in the incubation.

918 Finally, the gels were stained with Coomassie Brilliant Blue R-250. To evaluate the
919 impact of pH, additional experiments were conducted by incubating the gels at 37°C for
920 48 hours in reaction buffers with varying pH values: 3.5, 5.5, 7.0, and 9.0.
921 Building on the proteomic evidence of GP63 expression in *T. rangeli* [18], we
922 conducted further analyses of the raw MS/MS data from the surface-enriched protein
923 fraction (SEP) of *T. rangeli* SC58 strain for detailed identification of GP63 expression.
924 This analysis employed MSFragger [137] and, also incorporated unpublished, in-house
925 generated secretome datasets from *T. rangeli*.
926 The final dataset comprises all 11 GP63 sequences, supplemented with
927 contaminant proteins from cRAP (https://thegp_m.org/crap/index.html), including
928 porcine trypsin, *Saccharomyces* spp. alcohol dehydrogenase, and human keratin.
929 Decoy database searches were performed automatically. MSFragger parameters
930 specified tryptic peptides allowing one missed cleavage, carbamidomethylation of
931 cysteine, methionine oxidation as a variable modification, and precursor and fragment
932 tolerances of 10 and 5 p.p.m., respectively. Protein identification and scoring were
933 conducted using the ProteinProphet algorithm within Philosopher [138]. Only proteins
934 supported by at least two unique peptides, a false discovery rate (FDR) below 0.1%,
935 and peptide/protein probabilities exceeding 95% and 99%, respectively, were
936 considered as valid.
937
938 *5.4.2 Structural and functional analysis of T. rangeli metalloproteases*
939 To investigate the presence of metalloprotease activity in *T. rangeli*, we
940 conducted *in silico* structural and functional analyses of these proteins. Initially, we
941 generated 3D models of *T. rangeli* metalloproteases using AlphaFold 3 [139]. For
942 comparative purposes, we also obtained the model of the group 1 metalloprotease from
943 *T. cruzi* (TriTrypDB: C4B63_30g122). All models were generated using the default
944 parameters of AlphaFold 3, as outlined in its user guide. Quality assessment of the
945 model was carried out using the confidence scores provided by the program, including
946 pLDDT (per-residue confidence) and pTM (predicted template modelling). Specifically,
947 pTM values above 0.5 were considered indicative of adequate modelling, while values

948 above 0.8 reflected high predictive quality [139]. All generated models were visualized,
949 analysed, and figures were created using PyMOL v.2.5.0 (https://www.pymol.org/).
950 For the structural and functional analyses of metalloproteases, leishmanolysin - a
951 metalloprotease from *L. major* (PDB: 1LML) - was utilized as the control structure [37].
952 The structural analysis focused on the identification of the active site or zinc-binding
953 motif (HEXXHXXG[~60]H) located in helix B, which is a conserved characteristic of
954 metalloproteases, was evaluated [41,44]. Surface representations of the models were
955 created to identify the S1' pocket, a common feature of these proteins extensively
956 studied for its importance in interactions with various inhibitors [140]. The loop region
957 preceding helix B, located between antiparallel β-sheets in the N-terminal domain, was
958 examined due to its presence in the active site of the metalloproteases. Furthermore,
959 we assessed the structural similarities between the metalloprotease models of *T.*
960 *rangeli*, *T. cruzi* and the control *L. major* models through structural alignments. This
961 process was followed by RMSD (Root Mean Square Deviation) calculations for both the
962 overall protein and for helix B specifically, considering only the alpha carbons in each
963 case.
964 To evaluate the interaction potential of the modeled metalloprotease active sites
965 with ligands, the proteins were submitted to the P2Rank web server [42]. P2Rank is a
966 machine-learning tool that identifies potential binding sites by analysing surface
967 features, shape, and electrostatic potential. The server provides a ranked list of
968 potential binding sites, derived from the P2Rank score and the ligand cavity probability.
969 The metalloprotease models were categorized into three groups based on the ligand
970 cavity probability value: (i) highly promising, when probability is ≥ 50%; (ii) moderately
971 promising, when it falls between < 50% and ≥ 40%; and (iii) less promising, when it is <
972 40%.
973 The metalloprotease models underwent molecular docking with 1,10-
974 phenanthroline, an established inhibitor of metalloproteinases [38,44]. This compound
975 typically interacts with the active site of these enzymes, specifically targeting the $Zn^{2+}$
976 ion, which serves as an indicator of a catalytic environment comparable to that of
977 metalloproteinases. Docking simulations were carried out using AutoDock Vina [141].
978 An optimized grid box was strategically positioned over the active site to generate nine

979 poses for each protein, while all other parameters adhered to the program's default
980 settings. Initially, the control structure was docked with 1,10-phenanthroline, and the
981 pose with the lowest affinity value and the most favourable orientation toward the $Zn^{2+}$
982 ion was selected as the reference model. Subsequently, docking was conducted with
983 the metalloproteases from *T. rangeli* and *T. cruzi*, focusing on poses that displayed the
984 highest similarity to the control complex. To accomplish this, the proteins were aligned,
985 and the RMSD between the ligands was calculated, with the pose showing the lowest
986 RMSD chosen for further analysis.
987
988 *5.4.3 T. rangeli mucin-like glycoproteins*
989 Identification of *T. rangeli* mucin-like glycoproteins was carried out by BLASTn
990 using the first 93 nt of *T. rangeli* mucin-likes TRSC58_06796 (TriTrypDB) and
991 KC544919 (GenBank) genes described in the reference genome [5] and proteome [18],
992 respectively. Also, the presence of N- and C-terminal domains of *T. cruzi* mucin-like
993 genes signatures [142,143] was assessed. Hits that did not match to a CDS
994 automatically annotated were evaluated by analysis ORFs obtained from 3 Kbp flanking
995 regions of identified hits using the GetORF tool (https://www.bioinformatics.nl/cgi-
996 bin/emboss/getorf), considering the following parameters: 150 nt minimum length; and
997 only Met as start codon. Only sequences encoding for valid signal peptides according to
998 SignalP v.6.0 predictor [128] or DeepTMHMM v.1.0 [129] were considered as putative
999 *T. rangeli* mucins (*Tr*MUC). The presence of GPI-anchor, *N*- and *O*-glycosylation sites,
1000 in addition to phosphorylation (ATM, CKI, CKII, CaM-II, DNAPK, EGFR, GSK3, INSR,
1001 PKA, PKB, PKC, PKG, RSK, SRC, cdc2, cdk5, and p38MAPK) recognition sites was
1002 evaluated using NetGPI v.1.1 [130], NetN-Glyc v.1.0, NetO-glyc v.4.0 [144], and
1003 NetPhos v.3.1 [145] servers, respectively. Prediction of amino acid abundance and
1004 molecular weight was performed by Pepstats tool available at EMBL-EBI Job
1005 Dispatcher [135]. The conservative regions were evaluated by Gblocks [146] applying
1006 Clustal Omega [147] alignments as inputs, as well as to obtain logos representations
1007 through the Skylign tool [148], and overall similarity analysis performed by SIAS tool.
1008 Phylogenetic analysis based on maximum-likelihood tree inferred amino acid sequences
1009 identified from the *T. rangeli* SC58 V.2 genome, as well as members of the *T. cruzi*

1010 mucin-like (MUC) and Trypomastigote Alanine-Serine-Valine (TASV) glycoprotein
1011 families retrieved from TryTripDB and Genbank databases was conducted as described
1012 for GP63 analysis.
1013
1014 *5.4.4 Biological assessment of T. rangeli mucins and TASV*
1015 We designed a synthetic gene (purchased from Biomatik) hereby called 'FlagGPI'
1016 encoding a 3xFlagTag® (Sigma-Aldrich) sequence, followed by the mNeonGreen
1017 fluorescent protein gene [149], and a *T. rangeli* GPI-anchor sequence (KC544919-
1018 GenBank) under control of *T. cruzi* gp82 3' untranslated region (UTR). The GFP gene
1019 present in the integrative plasmid pROCK-Neo [150] was replaced by the FlagGPI gene
1020 through *Xba*I and *Xho*I restriction enzyme cleavage, generating the FlagGPI-pROCK
1021 vector.
1022 The *T. rangeli* (Choachí strain) genes MUCg3 and TASV-like1, and the *T. cruzi*
1023 (Y strain) genes MUC I (clone B4-5), and MUC II (clone B2-10), were PCR amplified
1024 from genomic DNA. The amplicons, that excluded the GPI-anchor addition sequence,
1025 were gel purified using the QIAquick Purification kit (Qiagen), cloned in pGEM T-Easy
1026 vectors (Promega), sequenced (ABI3500 - Applied Biosystems), and subcloned in the
1027 FlagGPI-pROCK vector, resulting in tagged-fused constructs. A complete list of primers
1028 and restriction enzymes is provided in Additional file 15: Supplementary Table S8.
1029 Epimastigotes of *T. rangeli* (Choachí strain) were transfected with 10 µg of *Not*I-
1030 linearized FlagGPI-pROCK vector containing the distinct tagged-fused constructs or
1031 with the FlagGPI synthetic gene, using the Nucleofactor® II (Lonza) U-33 program. The
1032 transfected parasites were cultivated in LIT+NNN and selection was performed by
1033 increasing concentrations of geneticin (G418) up to 500 µg/mL. Plasmid integration into
1034 the parasite β-tubulin locus was confirmed by PCR using a set of primers designed to
1035 anneal exclusively in the genomic β-tubulin region upstream of the homologous
1036 recombination site and the HX1 5' UTR present particularly in FlagGPI-pROCK vector
1037 (Additional file 15: Supplementary Table S8). Once the integration into the parasite
1038 genome was confirmed, parasites were cultivated in the absence of selective drugs.
1039 To assess the expression of the FlagGPI-fused glycoproteins, total protein
1040 extracts of *T. rangeli* epimastigotes and trypomastigotes from each transfected lineage

1041 and wild-type parasites were obtained by lysis in proper buffer (50 mM NaCl, 200 mM
1042 Tris-HCl pH 8.0, 1% (v/v) Triton X-100), supplemented with a protease inhibitor cocktail
1043 (Sigma-Aldrich). A total of 50 µg of each extract were resolved in 12% SDS-Page gels
1044 and then wet-transferred to Hybond® PVDF membranes (Amersham). Membranes were
1045 incubated with primary antibodies (mouse anti-FlagTag M2 or rabbit anti-β-tubulin), then
1046 with HRP anti-IgG conjugates (anti-mouse or anti-rabbit) (Sigma-Aldrich). The
1047 expression analysis was periodically assessed.

1048 Comparative *in vivo* assessment of the infectivity of all transfected lineages was
1049 performed using 6 weeks old female BALB/c mice, maintained in ventilated cages under
1050 a 12-hour light/dark cycle and having water and food *ad libitum*. A total $1x10^7$ *in vitro*
1051 differentiated *T. rangeli* trypomastigotes were injected by intraperitoneal (i.p.) route and
1052 parasitemia was assessed daily by the Pizzi-Brener method from 6h post-infection
1053 [151]. *In vivo* experiments were approved by the UFSC Animal Ethics Committee
1054 (Protocol 9923170516). Graph and statistical analysis were performed using GraphPad
1055 Prism v.8.4.0 software. The expression of *T. rangeli* mucins and TASV was also
1056 evaluated by search on *T. rangeli* MS/MS proteomic data as performed for GP63 (Item
1057 2.4.1.).

1058

1059 *5.5 Analysis of orthologous groups*

1060 Orthology analysis was performed with OrthoFinder v.2.3.11 [152] using the
1061 predicted proteins from *T. rangeli* SC58 V.2 genome and proteins from *T. brucei*
1062 (TREU927 strain), *T. cruzi* (CL Brener Esmeraldo-like and Sylvio X10/1 strains), *T.*
1063 *rangeli* (SC58 reference strain), *Leishmania amazonensis* (MHOM/BR/71973/M2269
1064 strain) and *Leishmania infantum* (JPCM5 strain), obtained from TriTrypDB version 65
1065 [115], and also *T. rangeli* (AM80 strain) retrieved from GenBank (Access code:
1066 GCF_003719475.1).

1067

1068 *5.6 Comparative intra-specific genomics of T. rangeli strains*

1069 Illumina paired-end libraries of distinct *T. rangeli* strains (SC58, Choachí, PIT10,
1070 and R1625) were quality-filtered using Trimmomatic v0.40 [101] and the filtered reads

1071 were mapped against the *T. rangeli* SC58 V.2 genome using the Burrows-Wheeler
1072 Aligner v. 0.7.17 [153].
1073 For SNP calling, the mapping files were sorted with Samtools v.1.17 [154], PCR-
1074 duplicates were marked with Picard v.2.27.5 (http://broadinstitute.github.io/picard/), and
1075 SNPs were identified using the Genome Analysis Toolkit v.3.8
1076 (https://gatk.broadinstitute.org/hc/en-us) using the "HaplotypeCaller" algorithm with a
1077 minimum quality value of 30 and a minimum depth of coverage of 10. A strict mapping
1078 quality filter was applied to remove the influence of low mapping quality in repeated
1079 regions and any SNP with mapping quality <50 was removed using BCFtools v.1.9
1080 [154].
1081 CCNV and ploidy estimation were performed using a combination of RDC and
1082 AB methods as previously described [36]. Briefly, the estimation of CCNV was based on
1083 the ratio between the mean coverage in each *T. rangeli* SC58 V.2 scaffold and the
1084 mean coverage of all scaffolds in the assembly. If the ratio between the median
1085 chromosome coverage and the median genome coverage was approximately one, the
1086 chromosome had the same copy as the genome overall, while fluctuations in this ratio
1087 (<0.75 or >1.25) were considered as putative aneuploidies. Heterozygous SNPs with a
1088 mapping quality higher than 50 were selected for AB analyses to confirm aneuploidies
1089 and to estimate chromosome somy and whole genome ploidy. Whole genome ploidy
1090 was estimated by analysing the proportion of the alleles in heterozygous SNP positions
1091 of all scaffolds. To confirm the RDC somy estimations, the proportion of each allele with
1092 heterozygous SNPs per chromosome position was plotted for the 82 scaffolds. All RDC
1093 and AB graphs were generated in R with ggplot2 (available at
1094 https://ggplot2.tidyverse.org), pheatmap (available at https://CRAN.R-
1095 project.org/package=pheatmap), and vcfR [155] packages. Gene Ontology Enrichment
1096 analyses in CCNV regions were performed using TriTryp tools
1097 (https://tritrypdb.org/tritrypdb/app/) based on orthologs with the *T. cruzi* reference CL
1098 Brener Esmeraldo-like.
1099
1100 **ADDITIONAL FILES**

1101 **Additional file 1: Supplementary Figure S1**. Comparative alignment of the
1102 assemblies of *Trypanosoma rangeli* SC58 V.2 genome with other *T. rangeli* and *T. cruzi*
1103 genomes.
1104
1105 Footnote: Dot-plot representation of the alignment of the *T. rangeli* SC58 V.2 genome assembly with the
1106 reference genome (A), *T. rangeli* Choachí (B), PIT10 strain (C) and R1625 (D) strains genomes, *T. cruzi*
1107 CL Brener Esmeraldo-like (E), and Sylvio X10/1 strains genomes using comparative dot-plots generated
1108 by D-Genies (Cabanettes et al., 2018).
1109
1110 **Additional file 2: Supplementary Figure S2.** *Trypanosoma rangeli* five loci of the
1111 Spliced Leader RNA genes interspersed with 5S RNA genes.
1112
1113 Footnote: (**A**) Alignment of 62 *T. rangeli* Spliced-Leader (SL) RNA genes highlight the exon region (light
1114 green), intron (light red), and splicing site at position 39. (**B**) Five loci show SL genes interspersed with 5S
1115 RNA genes, varying from 9 to 16 SL gene copies.
1116
1117 **Additional file 3: Supplementary Table S1**. Mapping of *Trypanosoma cruzi* (CL
1118 Brener strain) chromosome-specific probes onto the *Trypanosoma rangeli* SC58 V.2
1119 genome.
1120
1121 Footnote: *Access codes of *T. cruzi* genes in the TriTrypDB v.65 database. **Genomic location and "P"
1122 and "S" haplotypes of *T. cruzi* CL Brener genome (Weatherly; Boehlke; Tarleton, 2009).
1123
1124 **Additional file 4: Supplementary Table S2**. Telomeric regions identified in the
1125 *Trypanosoma rangeli* SC58 V.2 genome scaffolds.
1126
1127 Footnote: bp = base pairs.
1128
1129 **Additional file 5: Supplementary Figure S3 -** Allelic proportions at heterozygous SNP
1130 positions for the 81 scaffolds of each *Trypanosoma rangeli* strain (SC58, Choachí,
1131 PIT10, R1625). Blue points represent allele proportions along each scaffold; black lines
1132 indicate median values within sliding windows.

1133

1134 **Additional file 6: Supplementary Table S3**. Summary of GP63 genes of *T. rangeli* and
1135 other Kinetoplastids species are presented in the phylogenetic analysis.

1136

1137 Footnote: 'GPI-Anchored' in red= sequence forecasted as GPI-anchored, however biologically not
1138 possible if signal peptide prediction is correct. 'BNP' = biologically not possible; SP = Signal Peptide;
1139 GLOB = globular; TM = transmembrane, ----- = presence of gap in active site region; XXxxX = Non-
1140 conserved amino acids in zinc-binding site/active site (other than HExxH). NE: Non-evaluated.
1141 Peptidase_M8 Superfamily (NCBI CDD code: cl19482).

1142

1143 **Additional file 7: Supplementary Figure S4.** *Trypanosoma rangeli* Surface
1144 Glycoprotein 63 (GP63) presents the main classical leishmanolysin motifs.

1145

1146 Footnote: Logo representation of residue conservation as weighted counts of Zinc-binding site. Logo Y-
1147 axis = observed information content (in bits), top = residues position in the alignment; bottom =
1148 occupancy values.

1149

1150 **Additional file 8: Supplementary Table S4**. Amino Acid Percent Identity Matrix of
1151 *Tr*GP63 complete genes.

1152

1153 Footnote: Colors highlight the *Tr*GP63 groups categorization as shown in the header of the matrix.

1154

1155 **Additional file 9: Supplementary Figure S5.** *Trypanosoma rangeli* exhibits
1156 metalloprotease activity, and it is biochemically inhibited by chelating agents.

1157

1158 Footnote: (**A**) Total protein extracts from epimastigotes (E) and culture-derived trypomastigotes (T) of *T.*
1159 *rangeli* ($10^8$ cells) were analysed by SDS-PAGE (10%) using a 0.2% gelatin-containing gel, without
1160 heating or reducing the samples before electrophoresis. Gels were incubated at 37 °C for 48 h in reaction
1161 buffer, without (-) or with (+) specific inhibitor 1,10-phenanthroline. Proteolytic activity is visualized as
1162 clear bands against the Coomassie brilliant blue-stained gelatin background. (**B**) Total protein extracts
1163 from axenic forms of *T. rangeli* Choachí strain (Tr), *T. cruzi* Y strain (Tc), and promastigotes of *L.*
1164 *braziliensis* MHOM/BR/75/M2904 strain ($10^8$ cells) were analysed in gels incubated with reaction buffers
1165 at different pH conditions.

1166

1167 **Additional file 10: Supplementary Table S5**. Values from the structural and *in silico*
1168 functional analyses of *Trypanosoma rangeli* GP63 metalloproteases.
1169
1170 Footnote: Metalloprotease from *L. major* (PDB: 1LML) was used as a control, and a single-sequence from
1171 *T. cruzi* group 1 (TriTrypDB:C4B63_30g122) was included for comparative analysis. Colors indicate
1172 metalloprotease inferred activity based on ligand cavity scores: Green for highly promising (≥ 0.5), yellow
1173 for moderately promising (<0.5 to ≥ 0.4), and red for moderately promising (<0.4). pTM = predicted
1174 template modelling. RMSD = root mean square deviation.
1175
1176 **Additional file 11: Supplementary Figure S6.** Structure of *Trypanosoma rangeli* GP63
1177 metalloproteases from distinct groups.
1178
1179 Footnote: **(A)** Structural and *in silico* functional analysis of *T. rangeli* GP63 classified as a highly
1180 promising group regarding inferred activity. (**B**) *Tr*GP63 is classified as a moderately promising group. (**C**)
1181 *Tr*GP63 was predicted as a less promising group. 3D Model: Three-dimensional models demonstrating
1182 the region corresponding to the active/Zinc-binding site (Highlighted by a box), where structural and
1183 functional analyses were performed. Zinc-binding site: Visualization of the conserved amino acid residues
1184 are shown in stick representation. Molecular surface: representation of the proteins indicating the
1185 presence or absence of the S1' pocket representing the position which interacts with inhibitors. Presence
1186 of S1' pocket is indicated by a green arrow, and absence by a red arrow. P2Rank analysis: Ligand-cavity
1187 prediction shown by colours demonstrates different predicted cavity positions. Predicted binding cavity
1188 probability is shown in the boxes. Molecular docking analysis: Complexes of metalloproteases with the
1189 inhibitor 1,10-phenanthroline. The cyan ligand represents the highest-affinity conformation obtained for
1190 the control structure, while the white ligands correspond to molecular docking results for the other GP63.
1191 Blue indicates nitrogen in both representations. The boxes present the RMSD values (Å) and ΔG
1192 (kcal/mol) of the complexes resulting from molecular docking.
1193
1194 **Additional file 12: Supplementary Table S6**. Description of *Tr*MUC and *Tr*TASV
1195 genes and predicted glycoprotein characteristics.
1196
1197 Footnote: Yellow background= *T. rangeli* glycoproteins selected for biological characterization. "MW"=
1198 Molecular Weight marker, "WB"= Western Blot. *excluded mature FlagGPI construct 30.39 kDa. #GPI-
1199 anchor cleavage did not occur in the synthetic gene due to a lack of signal peptide. Aromatic residues
1200 (Phe, His, Trp, Tyr). NP = Non-provided by DeepTMHMM Signal peptide predictor.
1201

1202 **Additional file 13: Supplementary Figure S7:** Comparative parasitemia between wild-
1203 type *Trypanosoma rangeli* and transfectants expressing T*r*MUC, *Tr*TASV-like1, or
1204 *Tc*MUC genes.
1205
1206 Footnote: Graphs expressed as means and standard error of mean by lines and shaded regions,
1207 respectively. Statistical analysis: Normal distribution of data evaluated by Kolmogorov-Smirnov test
1208 (α=0.05), followed by two-way ANOVA and Post Hoc Bonferroni´s multiple comparisons test. Differences
1209 between groups per time point are shown in the graphs. Unique statistical symbols demonstrate the same
1210 statistical difference in all time points between 1 to 10 d.p.i. (ns $p>0.05$; *$p\leq0.05$; **$p\leq0.01$;*** $p\leq0.001$;
1211 **** $p\leq0.0001$). The overall evaluation between the transfected parasite lineages, regardless of time point,
1212 is provided in the detailed table.
1213
1214 **Additional file 14: Supplementary Table S7**. *Trypanosoma rangeli* strains used in this
1215 study, showing their original hosts and geographical origins, as well as their distinct
1216 genetic classifications based on kDNA and ribosomal markers.
1217
1218 Footnote: *kDNA-based classification as proposed by Vallejo et al. (2002). **Ribosomal markers-based (SSU and
1219 ITS) classification as proposed by Maia da Silva et al. (2004). ND= Not determined.
1220
1221 **Additional file 15: Supplementary Table S8:** Primers used in PCR amplification and
1222 cloning of *Trypanosoma rangeli* and *Trypanosoma cruzi* mucins into the FlagGPI-
1223 pROCK vector and on assessment of genomic integration.
1224
1225 Footnote: 'F' and 'R' stand for Forward and Reverse primers, respectively. Restriction sites are highlighted in
1226 bold/italics at the 5'-end of each primer sequence. *= Amplification product generated with primer HX1 R for
1227 integration evaluation by PCR.
1228
1229 **ABBREVIATIONS**
1230 AB: Allele Balance; Bp: Base pairs; CCNV: Chromosome Copy Number Variation; CDS: Coding
1231 sequence; DGF-1: Disperse Gene Family 1; GO: Gene Onthology; GP: Glycoprotein; GPI:
1232 Glycosylphosphatidylinositol; Kb: Kilobases; Kbp: Thousand base pairs; kcal/mol: Kilocalories per mole;
1233 kDa: Kilodaltons; KMP: Kinetoplastid Membrane Protein; mAb: Monoclonal antibody; MASP: Mucin-
1234 Associated Surface Proteins; Mb: Megabase; Mbp: Million base-pairs; pTM: Predicted template

modelling; RDC: Read Depth Coverage; RHS: Retrotransposon Hot Spot; RMSD: Root Mean Square Deviation; RNAi: RNA interference machinery; SNP: Single Nucleotide Polymorphism; TASV: Trypomastigote, Alanine, Serine and Valine rich protein glycoprotein family; VSG: Variable Surface Glycoprotein.

**ACKNOWLEDGMENTS**

The authors would like to thank the Laboratório de Estudos em Biologia (LAMEB/UFSC, Brazil) and the Science for Life Laboratory (KI, Stockholm) for technical support. Authors are indebted to Dr Ariel Silber (USP, Brazil) for critical reading and valuable comments on this manuscript.

**AUTHOR'S CONTRIBUTIONS**

GAM, GMM and ACS: Equally contributed to Formal analysis, Investigation, Methodology, Validation, Visualization and Writing – original draft.

CAP, CLMP, DDL, RAC, RSM and TKSP: Formal analysis, Investigation, Methodology and Validation. ASR: Formal analysis and Investigation.

TCB and GRM: Formal analysis, Investigation, Methodology, Validation and Writing – original draft.

JFSF, MS: Data curation, Formal analysis, Investigation, Resources, Supervision, Validation and Writing – original draft.

PHS and GW: Data curation, Formal analysis, Investigation, Methodology, Validation, Resources, Supervision and Writing – original draft.

BA and ECG: Conceptualization, Data curation, Formal analysis, Funding acquisition, Investigation, Project administration, Resources, Supervision, Validation and Writing – original draft.

**FUNDING**

This work was supported by grants from the following Brazilian Government Agencies: Conselho Nacional de Desenvolvimento Científico e Tecnológico - CNPq (Grants 477385/2012-5 and 308616/2015-4), Coordenação de Aperfeiçoamento de Pessoal de Nível Superior - CAPES (Grants CAPES/PRINT 88887.311315/2018-00 and CAPES/STINT 23038.003782/2014–11), Financiadora de Estudos e Projetos - FINEP

(Grant 0847/07); and from the Swedish Research Council - SRC (Grant 2021-05667). GAM, ACS, CLMP, DDL, ASR, TCB, and RAC were recipients of CNPq or CAPES scholarships.

## AVAILABILITY OF DATA AND MATERIALS

Data generated during the current study is available in the GenBank database (Bioproject PRJNA1380247). Further datasets or subsets used and/or analysed during the current study are available from the corresponding authors on reasonable request. DNA transfer from UFSC to KI was carried out exclusively for sequencing purposes and was registered in the Brazilian National System for the Management of Genetic Heritage and Associated Traditional Knowledge (SISGEN A206000).

## ETHICS APPROVAL AND CONSENT TO PARTICIPATE

Not applicable.

## CONSENT FOR PUBLICATION

Not applicable.

## COMPETING INTERESTS

The authors declare no competing interests. The funders had no role in the study design, data analysis, or the decision to publish.

## AUTHOR DETAILS

1- Departamento de Microbiologia, Imunologia e Parasitologia, Universidade Federal de Santa Catarina (UFSC), Florianópolis - SC, Brazil.
2- Department of Medical Biochemistry and Biophysics, Karolinska Institutet (KI), Stockholm, Sweden.
3- Department of Microbiology, Tumor and Cell Biology, Karolinska Institutet (KI), Stockholm, Sweden.
4- Departamento de Microbiologia, Imunobiologia e Parasitologia, Universidade Federal de São Paulo (UNIFESP), São Paulo - SP, Brazil.

5- Instituto Federal de Santa Catarina (IFSC), Gaspar - SC, Brazil.

6- Departamento de Bioquímica, Universidade Federal de Santa Catarina (UFSC), Florianópolis - SC, Brazil.

7- Department of Cell and Molecular Biology, Karolinska Institutet (KI), Stockholm, Sweden.

## REFERENCES

1. Horn D, Spence C, Ingram AK. Telomere maintenance and length regulation in Trypanosoma brucei. EMBO J. 2000;19:2332–9. https://doi.org/10.1093/emboj/19.10.2332

2. WHO WHO. Chagas disease (also known as American trypanosomiasis) [Internet]. 2025 [cited 2025 Aug 31]. https://www.who.int/news-room/fact-sheets/detail/chagas-disease-(american-trypanosomiasis). Accessed 31 Aug 2025

3. WHO WHO. Leishmaniasis [Internet]. 2023 [cited 2025 Aug 31]. https://www.who.int/news-room/fact-sheets/detail/leishmaniasis. Accessed 31 Aug 2025

4. Urdaneta-Morales S, Tejero F. Trypanosoma (Herpetosoma) rangeli Tejera, 1920: intracellular amastigote stages of reproduction in white mice. Rev Inst Med Trop Sao Paulo [Internet]. Instituto de Medicina Tropical de São Paulo; 1986;28:166–9. https://doi.org/10.1590/S0036-46651986000300005

5. Stoco PH, Wagner G, Talavera-Lopez C, Gerber A, Zaha A, Thompson CE, et al. Genome of the Avirulent Human-Infective Trypanosome—Trypanosoma rangeli. PLoS Negl Trop Dis. 2014;8:e3176. https://doi.org/10.1371/journal.pntd.0003176

6. Grisard EC, Steindel M, Guarneri AA, Eger-Mangrich I, Campbell DA, Romanha AJ. Characterization of Trypanosoma rangeli Strains Isolated in Central and South America: an Overview. Mem Inst Oswaldo Cruz. 1999;94:203–9. https://doi.org/10.1590/S0074-02761999000200015

7. Guhl F, Vallejo GA. Trypanosoma (Herpetosoma) rangeli Tejera, 1920: an updated review. Mem Inst Oswaldo Cruz. 2003;98:435–42. https://doi.org/10.1590/S0074-02762003000400001

8. Dario MA, Moratelli R, Schwabl P, Jansen AM, Llewellyn MS. Small subunit ribosomal metabarcoding reveals extraordinary trypanosomatid diversity in Brazilian bats. PLoS Negl Trop Dis. 2017;11:e0005790. https://doi.org/10.1371/journal.pntd.0005790

9. Duarte da Silva B, Guarneri AA. *Trypanosoma rangeli* infection impairs reproductive success of *Rhodnius prolixus*. Parasitology. 2023;150:42–8. https://doi.org/10.1017/S0031182022001470

10. Bayão T de S, Cupertino M do C, Mayers NAJ, Siqueira-Batista R. A systematic review of the diagnostic aspects and use of Trypanosoma rangeli as an immunogen for

Trypanosoma cruzi infection. Rev Soc Bras Med Trop. 2020;53. https://doi.org/10.1590/0037-8682-0608-2019

11. Dario MA, Pavan MG, Rodrigues MS, Lisboa CV, Kluyber D, Desbiez ALJ, et al. Trypanosoma rangeli Genetic, Mammalian Hosts, and Geographical Diversity from Five Brazilian Biomes. Pathogens. 2021;10:736. https://doi.org/10.3390/pathogens10060736

12. Cruz-Saavedra L, Ospina C, Gutiérrez SA, Jaimes-Dueñez J, Cantillo-Barraza O, Hernández C, et al. Exploring Trypanosoma cruzi transmission dynamics in an acute Chagas disease outbreak using next-generation sequencing. Parasit Vectors. 2024;17:395. https://doi.org/10.1186/s13071-024-06445-9

13. de Moraes MH, Guarneri AA, Girardi FP, Rodrigues JB, Eger I, Tyler KM, et al. Different serological cross-reactivity of Trypanosoma rangeli forms in Trypanosoma cruzi-infected patients sera. Parasit Vectors. 2008;1:20. https://doi.org/10.1186/1756-3305-1-20

14. Rodrigues ES, Santos GQ, Silva MV da, Barros JHS, Bernardo AR, Diniz RL, et al. Chagas Immunochromatographic Rapid Test in the Serological Diagnosis of Trypanosoma cruzi Infection in Wild and Domestic Canids. Front Cell Infect Microbiol. 2022;12. https://doi.org/10.3389/fcimb.2022.835383

15. Kann S, Concha G, Weinreich F, Hahn A, Rückert C, Kalinowski J, et al. Comparative Assessment of Two Commercial Real-Time PCR Assays for the Diagnosis of Trypanosoma cruzi DNA in Serum. Microorganisms. 2023;11:901. https://doi.org/10.3390/microorganisms11040901

16. Bradwell KR, Koparde VN, Matveyev A V, Serrano MG, Alves JMP, Parikh H, et al. Genomic comparison of Trypanosoma conorhini and Trypanosoma rangeli to Trypanosoma cruzi strains of high and low virulence. BMC Genomics. 2018;19:770. https://doi.org/10.1186/s12864-018-5112-0

17. Grisard EC, Stoco PH, Wagner G, Sincero TCM, Rotava G, Rodrigues JB, et al. Transcriptomic analyses of the avirulent protozoan parasite Trypanosoma rangeli. Mol Biochem Parasitol. 2010;174:18–25. https://doi.org/10.1016/j.molbiopara.2010.06.008

18. Wagner G, Yamanaka LE, Moura H, Lückemeyer DD, Schlindwein AD, Stoco PH, et al. The Trypanosoma rangeli trypomastigote surfaceome reveals novel proteins and targets for specific diagnosis. J Proteomics. 2013/03/08. 2013;82:52–63. https://doi.org/10.1016/j.jprot.2013.02.011

19. McGwire BS, Chang K-P, Engman DM. Migration through the Extracellular Matrix by the Parasitic Protozoan *Leishmania* Is Enhanced by Surface Metalloprotease gp63. Infect Immun. 2003;71:1008–10. https://doi.org/10.1128/IAI.71.2.1008-1010.2003

20. Berná L, Chiribao ML, Pita S, Alvarez-Valin F, Parodi-Talice A. Exploring the genomic landscape of the GP63 family in Trypanosoma cruzi: Evolutionary dynamics and functional peculiarities. PLoS Negl Trop Dis. 2025;19:e0012950. https://doi.org/10.1371/journal.pntd.0012950

21. Chiurillo MA, Peralta A, Ramírez JL. Comparative study of Trypanosoma rangeli and Trypanosoma cruzi telomeres. Mol Biochem Parasitol. 2002;120:305–8. https://doi.org/10.1016/S0166-6851(02)00005-1
22. El-Sayed NM, Myler PJ, Bartholomeu DC, Nilsson D, Aggarwal G, Tran A-N, et al. The Genome Sequence of *Trypanosoma cruzi* , Etiologic Agent of Chagas Disease. Science (1979). 2005;309:409–15. https://doi.org/10.1126/science.1112631
23. Talavera-López C, Messenger LA, Lewis MD, Yeo M, Reis-Cunha JL, Matos GM, et al. Repeat-Driven Generation of Antigenic Diversity in a Major Human Pathogen, Trypanosoma cruzi. Front Cell Infect Microbiol. 2021;11. https://doi.org/10.3389/fcimb.2021.614665
24. Herreros-Cabello A, Callejas-Hernández F, Gironès N, Fresno M. Trypanosoma Cruzi Genome: Organization, Multi-Gene Families, Transcription, and Biological Implications. Genes (Basel). 2020;11:1196. https://doi.org/10.3390/genes11101196
25. Reis-Cunha JL, Coqueiro-dos-Santos A, Pimenta-Carvalho SA, Marques LP, Rodrigues-Luiz GF, Baptista RP, et al. Accessing the Variability of Multicopy Genes in Complex Genomes using Unassembled Next-Generation Sequencing Reads: The Case of Trypanosoma cruzi Multigene Families. mBio. 2022;13. https://doi.org/10.1128/mbio.02319-22
26. Berná L, Rodriguez M, Chiribao ML, Parodi-Talice A, Pita S, Rijo G, et al. Expanding an expanded genome: long-read sequencing of Trypanosoma cruzi. Microb Genom. 2018;4. https://doi.org/10.1099/mgen.0.000177
27. Ghedin E, Bringaud F, Peterson J, Myler P, Berriman M, Ivens A, et al. Gene synteny and evolution of genome architecture in trypanosomatids. Mol Biochem Parasitol. 2004;134:183–91. https://doi.org/10.1016/j.molbiopara.2003.11.012
28. El-Sayed NM, Myler PJ, Blandin G, Berriman M, Crabtree J, Aggarwal G, et al. Comparative genomics of trypanosomatid parasitic protozoa. Science. 2005;309:404–9. https://doi.org/10.1126/science.1112181
29. Reis-Cunha JL, Bartholomeu DC. Trypanosoma cruzi Genome Assemblies: Challenges and Milestones of Assembling a Highly Repetitive and Complex Genome. 2019. p. 1–22. https://doi.org/10.1007/978-1-4939-9148-8_1
30. Müller LSM, Cosentino RO, Förstner KU, Guizetti J, Wedel C, Kaplan N, et al. Genome organization and DNA accessibility control antigenic variation in trypanosomes. Nature. 2018;563:121–5. https://doi.org/10.1038/s41586-018-0619-8
31. Vitarelli M de O, Franco TA, Pires D da S, Lima ARJ, Viala VL, Kraus AJ, et al. Integrating high-throughput analysis to create an atlas of replication origins in *Trypanosoma cruzi* in the context of genome structure and variability. mBio. 2024;15. https://doi.org/10.1128/mbio.00319-24
32. Ferreira L de L, Araújo FF de, Martinelli PM, Teixeira-Carvalho A, Alves-Silva J, Guarneri AA. New features on the survival of human-infective Trypanosoma rangeli in a

1414 murine model: Parasite accumulation is observed in lymphoid organs. PLoS Negl Trop
1415 Dis. 2020;14:e0009015. https://doi.org/10.1371/journal.pntd.0009015
1416 33. Medina-Acosta E, Franco AM, Jansen AM, Sampol M, Nevés N, Pontes-de-
1417 Carvalho L, et al. Trans-sialidase and sialidase activities discriminate between
1418 morphologically indistinguishable trypanosomatids. Eur J Biochem. 1994;225:333–9.
1419 https://doi.org/10.1111/j.1432-1033.1994.00333.x
1420 34. Pontes-de-Carvalho LC, Tomlinson S, Nussenzweig V. Trypanosoma rangeli
1421 sialidase lacks trans-sialidase activity. Mol Biochem Parasitol. 1993;62:19–25.
1422 https://doi.org/10.1016/0166-6851(93)90173-U
1423 35. Buschiazzo A. Structural basis of sialyltransferase activity in trypanosomal
1424 sialidases. EMBO J. 2000;19:16–24. https://doi.org/10.1093/emboj/19.1.16
1425 36. Matos GM, Lewis MD, Talavera-López C, Yeo M, Grisard EC, Messenger LA, et al.
1426 Microevolution of Trypanosoma cruzi reveals hybridization and clonal mechanisms
1427 driving rapid genome diversification. Elife. 2022;11. https://doi.org/10.7554/eLife.75237
1428 37. Schlagenhauf E, Etges R, Metcalf P. The crystal structure of the Leishmania major
1429 surface proteinase leishmanolysin (gp63). Structure. 1998;6:1035–46.
1430 https://doi.org/10.1016/S0969-2126(98)00104-X
1431 38. Guay-Vincent M-M, Matte C, Berthiaume A-M, Olivier M, Jaramillo M, Descoteaux
1432 A. Revisiting Leishmania GP63 host cell targets reveals a limited spectrum of
1433 substrates. PLoS Pathog. 2022;18:e1010640.
1434 https://doi.org/10.1371/journal.ppat.1010640
1435 39. Joshi PB, Kelly BL, Kamhawi S, Sacks DL, McMaster WR. Targeted gene deletion
1436 in Leishmania major identifies leishmanolysin (GP63) as a virulence factor. Mol
1437 Biochem Parasitol. 2002;120:33–40. https://doi.org/10.1016/S0166-6851(01)00432-7
1438 40. Yao C, Chen B, Kang Z, Liu Y, Qi X, Wang Q. Binding, selectivity and sequence
1439 recognition of matrix metalloproteinase-2 to oligopeptides. J Biomol Struct Dyn.
1440 2020;38:275–82. https://doi.org/10.1080/07391102.2019.1578694
1441 41. Varghese A, Chaturvedi SS, Fields GB, Karabencheva-Christova TG. A synergy
1442 between the catalytic and structural Zn(II) ions and the enzyme and substrate dynamics
1443 underlies the structure–function relationships of matrix metalloproteinase collagenolysis.
1444 JBIC Journal of Biological Inorganic Chemistry. 2021;26:583–97.
1445 https://doi.org/10.1007/s00775-021-01876-6
1446 42. Jendele L, Krivak R, Skoda P, Novotny M, Hoksza D. PrankWeb: a web server for
1447 ligand binding site prediction and visualization. Nucleic Acids Res. 2019;47:W345–9.
1448 https://doi.org/10.1093/nar/gkz424
1449 43. Cuevas IC, Cazzulo JJ, Sánchez DO. gp63 Homologues in *Trypanosoma cruzi* :
1450 Surface Antigens with Metalloprotease Activity and a Possible Role in Host Cell
1451 Infection. Infect Immun. 2003;71:5739–49. https://doi.org/10.1128/IAI.71.10.5739-
1452 5749.2003

1453 44. Nam KH. Structural analysis of metal chelation of the metalloproteinase thermolysin
1454 by 1,10-phenanthroline. J Inorg Biochem. 2021;215:111319.
1455 https://doi.org/10.1016/j.jinorgbio.2020.111319
1456 45. Caeiro LD, Alba-Soto CD, Rizzi M, Solana ME, Rodriguez G, Chidichimo AM, et al.
1457 The protein family TcTASV-C is a novel Trypanosoma cruzi virulence factor secreted in
1458 extracellular vesicles by trypomastigotes and highly expressed in bloodstream forms.
1459 PLoS Negl Trop Dis. 2018;12:1–26. https://doi.org/10.1371/journal.pntd.0006475
1460 46. Canepa GE, Mesias AC, Yu H, Chen X, Buscaglia CA, Cánepa GE, et al. Structural
1461 features affecting trafficking, processing, and secretion of Trypanosoma cruzi mucins. J
1462 Biol Chem. 2012/06/19. 2012;287:26365–76. https://doi.org/10.1074/jbc.M112.354696
1463 47. Di Noia JM, D'Orso I, Sánchez DO, Frasch ACC. AU-rich Elements in the 3′-
1464 Untranslated Region of a New Mucin-type Gene Family of Trypanosoma cruzi Confers
1465 mRNA Instability and Modulates Translation Efficiency. Journal of Biological Chemistry.
1466 2000;275:10218–27. https://doi.org/10.1074/jbc.275.14.10218
1467 48. García EA, Ziliani M, Agüero F, Bernabó G, Sánchez DO, Tekiel V. TcTASV: A
1468 novel protein family in Trypanosoma cruzi identified from a subtractive trypomastigote
1469 cDNA library. PLoS Negl Trop Dis. 2010;4. https://doi.org/10.1371/journal.pntd.0000841
1470 49. Díaz-Viraqué F, Pita S, Greif G, de Souza R de CM, Iraola G, Robello C. Nanopore
1471 Sequencing Significantly Improves Genome Assembly of the Protozoan Parasite
1472 Trypanosoma cruzi. Genome Biol Evol. 2019;11:1952–7.
1473 https://doi.org/10.1093/gbe/evz129
1474 50. Callejas-Hernández F, Gironès N, Fresno M. Genome Sequence of *Trypanosoma*
1475 *cruzi* Strain Bug2148. Genome Announc. 2018;6.
1476 https://doi.org/10.1128/genomeA.01497-17
1477 51. Wang W, Peng D, Baptista RP, Li Y, Kissinger JC, Tarleton RL. Strain-specific
1478 genome evolution in Trypanosoma cruzi, the agent of Chagas disease. PLoS Pathog.
1479 2021;17:e1009254. https://doi.org/10.1371/journal.ppat.1009254
1480 52. Ramirez JL. An Evolutionary View of Trypanosoma Cruzi Telomeres. Front Cell
1481 Infect Microbiol. 2020;9. https://doi.org/10.3389/fcimb.2019.00439
1482 53. Li B. Keeping Balance Between Genetic Stability and Plasticity at the Telomere and
1483 Subtelomere of Trypanosoma brucei. Front Cell Dev Biol. 2021;9.
1484 https://doi.org/10.3389/fcell.2021.699639
1485 54. Freitas LM, dos Santos SL, Rodrigues-Luiz GF, Mendes TAO, Rodrigues TS,
1486 Gazzinelli RT, et al. Genomic Analyses, Gene Expression and Antigenic Profile of the
1487 Trans-Sialidase Superfamily of Trypanosoma cruzi Reveal an Undetected Level of
1488 Complexity. PLoS One. 2011;6:e25914. https://doi.org/10.1371/journal.pone.0025914
1489 55. Borst P. Discontinuous Transcription and Antigenic Variation In Trypanosomes.
1490 Annu Rev Biochem. 1986;55:701–32.
1491 https://doi.org/10.1146/annurev.bi.55.070186.003413

1492 56. Mayer MG, Santos MG dos, Silva MFL da, Floeter-Winter LM. Footprints of a
1493 trypanosomatid RNA world: pre-small subunit rRNA processing by spliced leader
1494 addition trans-splicing. Mem Inst Oswaldo Cruz. 2012;107:522–31.
1495 https://doi.org/10.1590/S0074-02762012000400013
1496 57. Parsons M, Nelson RG, Agabian N. The trypanosome spliced leader small RNA
1497 gene family: stage-specific modification of one of several similar dispersed genes.
1498 Nucleic Acids Res. 1986;14:1703–17. https://doi.org/10.1093/nar/14.4.1703
1499 58. Añez-Rojas N, Peralta A, Crisante G, Rojas A, Añez N, Ramírez JL, et al.
1500 Trypanosoma rangeli expresses a gene of the group II trans-sialidase superfamily. Mol
1501 Biochem Parasitol. 2005;142:133–6. https://doi.org/10.1016/j.molbiopara.2005.03.012
1502 59. Berriman M, Ghedin E, Hertz-Fowler C, Blandin G, Renauld H, Bartholomeu DC, et
1503 al. The Genome of the African Trypanosome *Trypanosoma brucei*. Science (1979).
1504 2005;309:416–22. https://doi.org/10.1126/science.1112642
1505 60. Kawashita SY, da Silva C V., Mortara RA, Burleigh BA, Briones MRS. Homology,
1506 paralogy and function of DGF-1, a highly dispersed Trypanosoma cruzi specific gene
1507 family and its implications for information entropy of its encoded proteins. Mol Biochem
1508 Parasitol. 2009;165:19–31. https://doi.org/10.1016/j.molbiopara.2008.12.010
1509 61. Ramírez JL. The Elusive Trypanosoma cruzi Disperse Gene Protein Family (DGF-
1510 1). Pathogens. 2023;12:292. https://doi.org/10.3390/pathogens12020292
1511 62. Liao X, Hu K, Salhi A, Zou Y, Wang J, Gao X. msRepDB: a comprehensive
1512 repetitive sequence database of over 80 000 species. Nucleic Acids Res.
1513 2022;50:D236–45. https://doi.org/10.1093/nar/gkab1089
1514 63. KASHI Y, KING D. Simple sequence repeats as advantageous mutators in
1515 evolution. Trends in Genetics. 2006;22:253–9. https://doi.org/10.1016/j.tig.2006.03.005
1516 64. Hall JPJ, Wang H, Barry JD. Mosaic VSGs and the Scale of Trypanosoma brucei
1517 Antigenic Variation. PLoS Pathog. 2013;9:e1003502.
1518 https://doi.org/10.1371/journal.ppat.1003502
1519 65. Claessens A, Hamilton WL, Kekre M, Otto TD, Faizullabhoy A, Rayner JC, et al.
1520 Generation of Antigenic Diversity in Plasmodium falciparum by Structured
1521 Rearrangement of Var Genes During Mitosis. PLoS Genet. 2014;10:e1004812.
1522 https://doi.org/10.1371/journal.pgen.1004812
1523 66. Morel CM, Acharya T, Broun D, Dangi A, Elias C, Ganguly NK, et al. Health
1524 Innovation Networks to Help Developing Countries Address Neglected Diseases.
1525 Science (1979). 2005;309:401–4. https://doi.org/10.1126/science.1115538
1526 67. Maia da Silva F, Marcili A, Lima L, Cavazzana M, Ortiz PA, Campaner M, et al.
1527 Trypanosoma rangeli isolates of bats from Central Brazil: Genotyping and phylogenetic
1528 analysis enable description of a new lineage using spliced-leader gene sequences. Acta
1529 Trop. 2009;109:199–207. https://doi.org/10.1016/j.actatropica.2008.11.005

1530 68. Abrahim M, Machado E, Alvarez-Valín F, de Miranda AB, Catanho M. Uncovering
1531 Pseudogenes and Intergenic Protein-coding Sequences in TriTryps' Genomes. Genome
1532 Biol Evol. 2022;14. https://doi.org/10.1093/gbe/evac142
1533 69. Reis-Cunha JL, Valdivia HO, Bartholomeu DC. Gene and Chromosomal Copy
1534 Number Variations as an Adaptive Mechanism Towards a Parasitic Lifestyle in
1535 Trypanosomatids. Curr Genomics. 2018;19.
1536 https://doi.org/10.2174/1389202918666170911161311
1537 70. Schwabl P, Imamura H, Van den Broeck F, Costales JA, Maiguashca-Sánchez J,
1538 Miles MA, et al. Meiotic sex in Chagas disease parasite Trypanosoma cruzi. Nat
1539 Commun. 2019;10:3972. https://doi.org/10.1038/s41467-019-11771-z
1540 71. Bussotti G, Gouzelou E, Côrtes Boité M, Kherachi I, Harrat Z, Eddaikra N, et al.
1541 *Leishmania* Genome Dynamics during Environmental Adaptation Reveal Strain-Specific
1542 Differences in Gene Copy Number Variation, Karyotype Instability, and Telomeric
1543 Amplification. mBio. 2018;9. https://doi.org/10.1128/mBio.01399-18
1544 72. Negreira GH, de Groote R, Van Giel D, Monsieurs P, Maes I, de Muylder G, et al.
1545 The adaptive roles of aneuploidy and polyclonality in *Leishmania* in response to
1546 environmental stress. EMBO Rep. 2023;24. https://doi.org/10.15252/embr.202357413
1547 73. Grünebast J, Clos J. Leishmania: Responding to environmental signals and
1548 challenges without regulated transcription. Comput Struct Biotechnol J. 2020;18:4016–
1549 23. https://doi.org/10.1016/j.csbj.2020.11.058
1550 74. Cabrine-Santos M, Ferreira KAM, Tosi LRO, Lages-Silva E, Ramírez LE, Pedrosa
1551 AL. Karyotype variability in KP1(+) and KP1(−) strains of Trypanosoma rangeli isolated
1552 in Brazil and Colombia. Acta Trop. 2009;110:57–64.
1553 https://doi.org/10.1016/j.actatropica.2009.01.004
1554 75. Henriksson J, Solari A, Rydåker M, Sousa OE, Pettersson U. Karyotype variability in
1555 *Trypanosoma rangeli*. Parasitology. 1996;112:385–91.
1556 https://doi.org/10.1017/S0031182000066610
1557 76. Lye L-F, Owens K, Shi H, Murta SMF, Vieira AC, Turco SJ, et al. Retention and
1558 Loss of RNA Interference Pathways in Trypanosomatid Protozoans. PLoS Pathog.
1559 2010;6:e1001161. https://doi.org/10.1371/journal.ppat.1001161
1560 77. Reis-Cunha JL, Pimenta-Carvalho SA, Almeida L V., Coqueiro-dos-Santos A,
1561 Marques CA, Black JA, et al. Ancestral aneuploidy and stable chromosomal duplication
1562 resulting in differential genome structure and gene expression control in trypanosomatid
1563 parasites. Genome Res. 2024; https://doi.org/10.1101/gr.278550.123
1564 78. Valdivia HO, Scholte LLS, Oliveira G, Gabaldón T, Bartholomeu DC. The
1565 Leishmania metaphylome: a comprehensive survey of Leishmania protein phylogenetic
1566 relationships. BMC Genomics. 2015;16:887. https://doi.org/10.1186/s12864-015-2091-2
1567 79. Castro Neto AL, Brito ANALM, Rezende AM, Magalhães FB, de Melo Neto OP. In
1568 silico characterization of multiple genes encoding the GP63 virulence protein from
1569 Leishmania braziliensis: identification of sources of variation and putative roles in

1570 immune evasion. BMC Genomics. 2019;20:118. https://doi.org/10.1186/s12864-019-
1571 5465-z
1572 80. LaCount DJ, Gruszynski AE, Grandgenett PM, Bangs JD, Donelson JE. Expression
1573 and Function of the Trypanosoma brucei Major Surface Protease (GP63) Genes.
1574 Journal of Biological Chemistry. 2003;278:24658–64.
1575 https://doi.org/10.1074/jbc.M301451200
1576 81. Grandgenett PM, Otsu K, Wilson HR, Wilson ME, Donelson JE. A Function for a
1577 Specific Zinc Metalloprotease of African Trypanosomes. PLoS Pathog. 2007;3:e150.
1578 https://doi.org/10.1371/journal.ppat.0030150
1579 82. Choi JY, Chung E. Molecular Dynamics Simulations of Matrix Metalloproteinase 13
1580 and the Analysis of the Specificity Loop and the S1′−Site. Int J Mol Sci. 2023;24:10577.
1581 https://doi.org/10.3390/ijms241310577
1582 83. Matheoud D, Moradin N, Bellemare-Pelletier A, Shio MT, Hong WJ, Olivier M, et al.
1583 Leishmania Evades Host Immunity by Inhibiting Antigen Cross-Presentation through
1584 Direct Cleavage of the SNARE VAMP8. Cell Host Microbe. 2013;14:15–25.
1585 https://doi.org/10.1016/j.chom.2013.06.003
1586 84. Contreras I, Gómez MA, Nguyen O, Shio MT, McMaster RW, Olivier M. Leishmania-
1587 Induced Inactivation of the Macrophage Transcription Factor AP-1 Is Mediated by the
1588 Parasite Metalloprotease GP63. PLoS Pathog. 2010;6:e1001148.
1589 https://doi.org/10.1371/journal.ppat.1001148
1590 85. Brittingham A, Chen G, McGwire BS, Chang K-P, Mosser DM. Interaction of
1591 *Leishmania* gp63 with Cellular Receptors for Fibronectin. Infect Immun. 1999;67:4477–
1592 84. https://doi.org/10.1128/IAI.67.9.4477-4484.1999
1593 86. Santos ALS, Branquinha MH, D'Avila-Levy CM. The ubiquitous gp63-like
1594 metalloprotease from lower trypanosomatids: in the search for a function. An Acad Bras
1595 Cienc. 2006;78:687–714. https://doi.org/10.1590/S0001-37652006000400006
1596 87. Osorio Y, Travi BL, Palma GI, Saravia NG. Infectivity of Trypanosoma rangeli in a
1597 promonocytic mammalian cell line. Journal of Parasitology. 1995;81:687–93.
1598 https://doi.org/10.2307/3283955
1599 88. Bueren-Calabuig JA, Pierdominici-Sottile G, Roitberg AE. Unraveling the differences
1600 of the hydrolytic activity of Trypanosoma cruzi trans-sialidase and Trypanosoma rangeli
1601 sialidase: a quantum mechanics-molecular mechanics modeling study. J Phys Chem B.
1602 2014/05/13. 2014;118:5807–16. https://doi.org/10.1021/jp412294r
1603 89. Burle-Caldas G de A, dos Santos NSA, de Castro JT, Mugge FLB, Grazielle-Silva V,
1604 Oliveira AER, et al. Disruption of Active Trans-Sialidase Genes Impairs Egress from
1605 Mammalian Host Cells and Generates Highly Attenuated Trypanosoma cruzi Parasites.
1606 mBio. 2022;13. https://doi.org/10.1128/mbio.03478-21
1607 90. Caeiro LD, Masip YE, Rizzi M, Rodríguez ME, Pueblas Castro C, Sánchez DO, et
1608 al. The Trypanosoma cruzi TcTASV-C protein subfamily administrated with U-Omp19

1609 promotes a protective response against a lethal challenge in mice. Vaccine.
1610 2020;38:7645–53. https://doi.org/10.1016/j.vaccine.2020.10.006
1611 91. Bernabó G, Levy G, Ziliani M, Caeiro LD, Sánchez DO, Tekiel V. TcTASV-C, a
1612 Protein Family in Trypanosoma cruzi that Is Predominantly Trypomastigote-Stage
1613 Specific and Secreted to the Medium. PLoS One. 2013;8:1–10.
1614 https://doi.org/10.1371/journal.pone.0071192
1615 92. Floridia-Yapur N, Monje Rumi M, Ragone P, Lauthier J, Tomasini N, Alberti
1616 D'Amato A, et al. The TcTASV proteins are novel promising antigens to detect active
1617 *Trypanosoma cruzi* infection in dogs. Parasitology. 2016;143:1382–9.
1618 https://doi.org/10.1017/S0031182016000822
1619 93. Queiroz RML, Charneau S, Bastos IMD, Santana JM, Sousa M V., Roepstorff P, et
1620 al. Cell Surface Proteome Analysis of Human-Hosted *Trypanosoma cruzi* Life Stages. J
1621 Proteome Res. 2014;13:3530–41. https://doi.org/10.1021/pr401120y
1622 94. Acosta-Serrano A. The mucin-like glycoprotein super-family of Trypanosoma cruzi:
1623 structure and biological roles. Mol Biochem Parasitol. 2001;114:143–50.
1624 https://doi.org/10.1016/S0166-6851(01)00245-6
1625 95. Campo VA, Buscaglia CA, Di Noia JM, Frasch ACC. Immunocharacterization of the
1626 mucin-type proteins from the intracellular stage of Trypanosoma cruzi. Microbes Infect.
1627 2006;8:401–9. https://doi.org/10.1016/j.micinf.2005.07.008
1628 96. Santos LF, Rocha F de S, Lorenzo MG, Guarneri AA. Revisiting the development of
1629 Trypanosoma rangeli in the vertebrate host. Mem Inst Oswaldo Cruz. 2024;119.
1630 https://doi.org/10.1590/0074-02760240138
1631 97. Frevert U, Schenkman S, Nussenzweig V. Stage-specific expression and
1632 intracellular shedding of the cell surface trans-sialidase of Trypanosoma cruzi. Infect
1633 Immun. 1992;60:2349–60. https://doi.org/10.1128/iai.60.6.2349-2360.1992
1634 98. Buschiazzo A, Campetella O, Frasch ACC. Trypanosoma rangeli sialidase: Cloning,
1635 expression and similarity to T. cruzi trans-sialidase. Glycobiology. 1998/02/10.
1636 1997;7:1167–73. https://doi.org/10.1093/glycob/7.8.1167
1637 99. Jers C, Michalak M, Larsen DM, Kepp KP, Li H, Guo Y, et al. Rational design of a
1638 new Trypanosoma rangeli trans-sialidase for efficient sialylation of glycans. PLoS One.
1639 2014/01/10. 2014;9:e83902. https://doi.org/10.1371/journal.pone.0083902
1640 100. Vallejo GA, Guhl F, Carranza JC, Lozano LE, Sánchez JL, Jaramillo JC, et al.
1641 kDNA markers define two major Trypanosoma rangeli lineages in Latin-America. Acta
1642 Trop. 2002;81:77–82. https://doi.org/10.1016/S0001-706X(01)00186-3
1643 101. Bolger AM, Lohse M, Usadel B. Trimmomatic: a flexible trimmer for Illumina
1644 sequence data. Bioinformatics. 2014;30:2114–20.
1645 https://doi.org/10.1093/bioinformatics/btu170
1646 102. Koren S, Walenz BP, Berlin K, Miller JR, Bergman NH, Phillippy AM. Canu:
1647 scalable and accurate long-read assembly via adaptive *k* -mer weighting and repeat
1648 separation. Genome Res. 2017;27:722–36. https://doi.org/10.1101/gr.215087.116

1649 103. Boetzer M, Henkel C V., Jansen HJ, Butler D, Pirovano W. Scaffolding pre-
1650 assembled contigs using SSPACE. Bioinformatics. 2011;27:578–9.
1651 https://doi.org/10.1093/bioinformatics/btq683
1652 104. Boetzer M, Pirovano W. Toward almost closed genomes with GapFiller. Genome
1653 Biol. 2012;13:R56. https://doi.org/10.1186/gb-2012-13-6-r56
1654 105. Walker BJ, Abeel T, Shea T, Priest M, Abouelliel A, Sakthikumar S, et al. Pilon: An
1655 Integrated Tool for Comprehensive Microbial Variant Detection and Genome Assembly
1656 Improvement. PLoS One. 2014;9:e112963.
1657 https://doi.org/10.1371/journal.pone.0112963
1658 106. Roach MJ, Schmidt SA, Borneman AR. Purge Haplotigs: allelic contig
1659 reassignment for third-gen diploid genome assemblies. BMC Bioinformatics.
1660 2018;19:460. https://doi.org/10.1186/s12859-018-2485-7
1661 107. Gurevich A, Saveliev V, Vyahhi N, Tesler G. QUAST: quality assessment tool for
1662 genome assemblies. Bioinformatics. 2013;29:1072–5.
1663 https://doi.org/10.1093/bioinformatics/btt086
1664 108. Marçais G, Delcher AL, Phillippy AM, Coston R, Salzberg SL, Zimin A. MUMmer4:
1665 A fast and versatile genome alignment system. PLoS Comput Biol. 2018;14:e1005944.
1666 https://doi.org/10.1371/journal.pcbi.1005944
1667 109. Camacho C, Coulouris G, Avagyan V, Ma N, Papadopoulos J, Bealer K, et al.
1668 BLAST+: architecture and applications. BMC Bioinformatics. 2009;10:421.
1669 https://doi.org/10.1186/1471-2105-10-421
1670 110. Manni M, Berkeley MR, Seppey M, Zdobnov EM. BUSCO: Assessing Genomic
1671 Data Quality and Beyond. Curr Protoc. 2021;1. https://doi.org/10.1002/cpz1.323
1672 111. Weatherly DB, Boehlke C, Tarleton RL. Chromosome level assembly of the hybrid
1673 Trypanosoma cruzi genome. BMC Genomics. 2009;10:255.
1674 https://doi.org/10.1186/1471-2164-10-255
1675 112. Maia GA, Filho VB, Kawagoe EK, Teixeira Soratto TA, Moreira RS, Grisard EC, et
1676 al. AnnotaPipeline: An integrated tool to annotate eukaryotic proteins using multi-omics
1677 data. Front Genet. 2022;13. https://doi.org/10.3389/fgene.2022.1020100
1678 113. Stanke M, Waack S. Gene prediction with a hidden Markov model and a new
1679 intron submodel. Bioinformatics. 2003;19:ii215–25.
1680 https://doi.org/10.1093/bioinformatics/btg1080
1681 114. Bateman A, Martin M-J, Orchard S, Magrane M, Agivetova R, Ahmad S, et al.
1682 UniProt: the universal protein knowledgebase in 2021. Nucleic Acids Res.
1683 2021;49:D480–9. https://doi.org/10.1093/nar/gkaa1100
1684 115. Amos B, Aurrecoechea C, Barba M, Barreto A, Basenko EY, Bażant W, et al.
1685 VEuPathDB: the eukaryotic pathogen, vector and host bioinformatics resource center.
1686 Nucleic Acids Res. 2022;50:D898–911. https://doi.org/10.1093/nar/gkab929

116. Jones P, Binns D, Chang H-Y, Fraser M, Li W, McAnulla C, et al. InterProScan 5: genome-scale protein function classification. Bioinformatics. 2014;30:1236–40. https://doi.org/10.1093/bioinformatics/btu031
117. Bray NL, Pimentel H, Melsted P, Pachter L. Near-optimal probabilistic RNA-seq quantification. Nat Biotechnol. 2016;34:525–7. https://doi.org/10.1038/nbt.3519
118. Eng JK, Jahan TA, Hoopmann MR. Comet: An open-source <scp>MS</scp> / <scp>MS</scp> sequence database search tool. Proteomics. 2013;13:22–4. https://doi.org/10.1002/pmic.201200439
119. The M, MacCoss MJ, Noble WS, Käll L. Fast and Accurate Protein False Discovery Rates on Large-Scale Proteomics Data Sets with Percolator 3.0. J Am Soc Mass Spectrom. 2016;27:1719–27. https://doi.org/10.1007/s13361-016-1460-7
120. Moreira RS, Benetti Filho V, Maia GA, Soratto TAT, Kawagoe EK, Russi BC, et al. FastProtein—an automated software for *in silico* proteomic analysis. PeerJ. 2024;12:e18309. https://doi.org/10.7717/peerj.18309
121. Kalvari I, Argasinska J, Quinones-Olvera N, Nawrocki EP, Rivas E, Eddy SR, et al. Rfam 13.0: shifting to a genome-centric resource for non-coding RNA families. Nucleic Acids Res. 2018;46:D335–42. https://doi.org/10.1093/nar/gkx1038
122. Nawrocki EP, Eddy SR. Infernal 1.1: 100-fold faster RNA homology searches. Bioinformatics. 2013;29:2933–5. https://doi.org/10.1093/bioinformatics/btt509
123. Sweeney BA, Petrov AI, Burkov B, Finn RD, Bateman A, Szymanski M, et al. RNAcentral: a hub of information for non-coding RNA sequences. Nucleic Acids Res. 2019;47:D221–9. https://doi.org/10.1093/nar/gky1034
124. Smit AFA, Hubley R, Green P. RepeatMasker [Internet]. 2025 [cited 2025 Aug 18]. https://www.repeatmasker.org/. Accessed 18 Aug 2025
125. Brown MR, Manuel Gonzalez de La Rosa P, Blaxter M. tidk: a toolkit to rapidly identify telomeric repeats from genomic datasets. Bioinformatics. 2025;41. https://doi.org/10.1093/bioinformatics/btaf049
126. Shen W, Le S, Li Y, Hu F. SeqKit: A Cross-Platform and Ultrafast Toolkit for FASTA/Q File Manipulation. PLoS One. 2016;11:e0163962. https://doi.org/10.1371/journal.pone.0163962
127. Waterhouse AM, Procter JB, Martin DMA, Clamp M, Barton GJ. Jalview Version 2—a multiple sequence alignment editor and analysis workbench. Bioinformatics. 2009;25:1189–91. https://doi.org/10.1093/bioinformatics/btp033
128. Nielsen H, Teufel F, Brunak S, von Heijne G. SignalP: The Evolution of a Web Server. 2024. p. 331–67. https://doi.org/10.1007/978-1-0716-4007-4_17
129. Hallgren J, Tsirigos KD, Pedersen MD, Almagro Armenteros JJ, Marcatili P, Nielsen H, et al. DeepTMHMM predicts alpha and beta transmembrane proteins using deep neural networks. 2022. https://doi.org/10.1101/2022.04.08.487609

130. Gíslason MH, Nielsen H, Almagro Armenteros JJ, Johansen AR. Prediction of GPI-anchored proteins with pointer neural networks. Curr Res Biotechnol. 2021;3:6–13. https://doi.org/10.1016/j.crbiot.2021.01.001
131. Button LL, Russell DG, Klein HL, Medina-Acosta E, Karess RE, McMaster WR. Genes encoding the major surface glycoprotein in Leishmania are tandemly linked at a single chromosomal locus and are constitutively transcribed. Mol Biochem Parasitol. 1989;32:271–83. https://doi.org/10.1016/0166-6851(89)90076-5
132. Rogers MB, Hilley JD, Dickens NJ, Wilkes J, Bates PA, Depledge DP, et al. Chromosome and gene copy number variation allow major structural change between species and strains of *Leishmania*. Genome Res. 2011;21:2129–42. https://doi.org/10.1101/gr.122945.111
133. Lemoine F, Correia D, Lefort V, Doppelt-Azeroual O, Mareuil F, Cohen-Boulakia S, et al. NGPhylogeny.fr: new generation phylogenetic services for non-specialists. Nucleic Acids Res. 2019;47:W260–5. https://doi.org/10.1093/nar/gkz303
134. Letunic I, Bork P. Interactive Tree Of Life (iTOL) v4: recent updates and new developments. Nucleic Acids Res [Internet]. 2019;47:W256–9. https://doi.org/10.1093/nar/gkz239
135. Madeira F, Madhusoodanan N, Lee J, Eusebi A, Niewielska A, Tivey ARN, et al. The EMBL-EBI Job Dispatcher sequence analysis tools framework in 2024. Nucleic Acids Res. 2024;52:W521–5. https://doi.org/10.1093/nar/gkae241
136. Sigrist CJA, de Castro E, Cerutti L, Cuche BA, Hulo N, Bridge A, et al. New and continuing developments at PROSITE. Nucleic Acids Res. 2012;41:D344–7. https://doi.org/10.1093/nar/gks1067
137. Kong AT, Leprevost F V, Avtonomov DM, Mellacheruvu D, Nesvizhskii AI. MSFragger: ultrafast and comprehensive peptide identification in mass spectrometry–based proteomics. Nat Methods. 2017;14:513–20. https://doi.org/10.1038/nmeth.4256
138. da Veiga Leprevost F, Haynes SE, Avtonomov DM, Chang H-Y, Shanmugam AK, Mellacheruvu D, et al. Philosopher: a versatile toolkit for shotgun proteomics data analysis. Nat Methods. 2020;17:869–70. https://doi.org/10.1038/s41592-020-0912-y
139. Abramson J, Adler J, Dunger J, Evans R, Green T, Pritzel A, et al. Accurate structure prediction of biomolecular interactions with AlphaFold 3. Nature. 2024;630:493–500. https://doi.org/10.1038/s41586-024-07487-w
140. Devel L, Czarny B, Beau F, Georgiadis D, Stura E, Dive V. Third generation of matrix metalloprotease inhibitors: Gain in selectivity by targeting the depth of the S1′ cavity. Biochimie. 2010;92:1501–8. https://doi.org/10.1016/j.biochi.2010.07.017
141. Trott O, Olson AJ. AutoDock Vina: Improving the speed and accuracy of docking with a new scoring function, efficient optimization, and multithreading. J Comput Chem. 2010;31:455–61. https://doi.org/10.1002/jcc.21334

142. Di Noia JM, D'Orso I, Aslund L, Sánchez DO, Frasch AC. The Trypanosoma cruzi mucin family is transcribed from hundreds of genes having hypervariable regions. J Biol Chem. 1998/06/06. 1998;273:10843–50. https://doi.org/10.1074/jbc.273.18.10843
143. Bartholomeu DC, Cerqueira GC, Leão ACA, daRocha WD, Pais FS, Macedo C, et al. Genomic organization and expression profile of the mucin-associated surface protein (masp) family of the human pathogen Trypanosoma cruzi. Nucleic Acids Res. 2009;37:3407–17. https://doi.org/10.1093/nar/gkp172
144. Steentoft C, Vakhrushev SY, Joshi HJ, Kong Y, Vester-Christensen MB, Schjoldager KT, et al. Precision mapping of the human O-GalNAc glycoproteome through SimpleCell technology. EMBO J. 2013/04/16. 2013;32:1478–88. https://doi.org/10.1038/emboj.2013.79
145. Blom N, Gammeltoft S, Brunak S. Sequence and structure-based prediction of eukaryotic protein phosphorylation sites. J Mol Biol. 1999;294:1351–62. https://doi.org/10.1006/jmbi.1999.3310
146. Castresana J. Selection of conserved blocks from multiple alignments for their use in phylogenetic analysis. Mol Biol Evol. 2000/03/31. 2000;17:540–52. https://doi.org/10.1093/oxfordjournals.molbev.a026334
147. Sievers F, Higgins DG. Clustal omega. Curr Protoc Bioinformatics. 2014/12/17. 2014;48:3 13 1-16. https://doi.org/10.1002/0471250953.bi0313s48
148. Wheeler TJ, Clements J, Finn RD. Skylign: a tool for creating informative, interactive logos representing sequence alignments and profile hidden Markov models. BMC Bioinformatics. 2014;15:7. https://doi.org/10.1186/1471-2105-15-7
149. Shaner NC, Lambert GG, Chammas A, Ni Y, Cranfill PJ, Baird MA, et al. A bright monomeric green fluorescent protein derived from Branchiostoma lanceolatum. Nat Methods [Internet]. 2013;10:407–9. https://doi.org/10.1038/nmeth.2413
150. DaRocha WD, Silva RA, Bartholomeu DC, Pires SF, Freitas JM, Macedo AM, et al. Expression of exogenous genes in Trypanosoma cruzi : improving vectors and electroporation protocols. Parasitol Res. 2004;92:113–20. https://doi.org/10.1007/s00436-003-1004-5
151. de Araújo-Jorge TC, de Castro SL. Doença de chagas: manual para experimentação animal. Doença de chagas: manual para experimentação animal. 2000. https://doi.org/10.7476/9788575413937
152. Emms DM, Kelly S. OrthoFinder: phylogenetic orthology inference for comparative genomics. Genome Biol. 2019;20:238. https://doi.org/10.1186/s13059-019-1832-y
153. Li H, Durbin R. Fast and accurate short read alignment with Burrows–Wheeler transform. Bioinformatics. 2009;25:1754–60. https://doi.org/10.1093/bioinformatics/btp324
154. Li H, Handsaker B, Wysoker A, Fennell T, Ruan J, Homer N, et al. The Sequence Alignment/Map format and SAMtools. Bioinformatics. 2009;25:2078–9. https://doi.org/10.1093/bioinformatics/btp352

155. Knaus BJ, Grünwald NJ. <scp>vcfr</scp> : a package to manipulate and visualize variant call format data in R. Mol Ecol Resour. 2017;17:44–53. https://doi.org/10.1111/1755-0998.12549

| Metrics | *T. rangeli* | | *T. cruzi* | |
|---|---|---|---|---|
| | **SC58 V.2** | **SC58 Reference*** | **CL Brener Esmeraldo-like*** | **Sylvio X10/1*** |
| **Genome size (Mbp)** | 23.68 | 14.02 | 32.53 | 41.38 |
| **Number of scaffolds** | 81 | 7,433 | 41 | 47 |
| **G+C content (%)** | 53.30 | 53.26 | 50.38 | 51.57 |
| **Scaffolds > 50 Kbp** | 67 | 0 | 41 | 47 |
| **Longest scaffold (Mbp)** | 1.37 | 0.25 | 2.37 | 3.12 |
| **Scaffold N50** | 558,628 | 2,203 | 870,934 | 1,006,492 |
| **Scaffold L50** | 14 | 2,096 | 12 | 14 |
| ***N* bases / 100 Kbp** | 0 | 21.31 | 20,604.70 | 3,242.42 |
| **Number of rRNA** | 58 | 16 | 9 | ND |
| **Number of tRNA** | 73 | 120 | 55 | 65 |
| **Total number of CDS** | 9,203 | 7,475 | 9,039 | 18,643 |
| **Number of hypothetical CDS** | 3,067 | 5,075 | 4,260 | 13,760 |
| **Mean CDS size (aa)** | 505 | 460 | 493 | 178 |
| **CDS < 100 aa** | 299 | 410 | 207 | 5,573 |

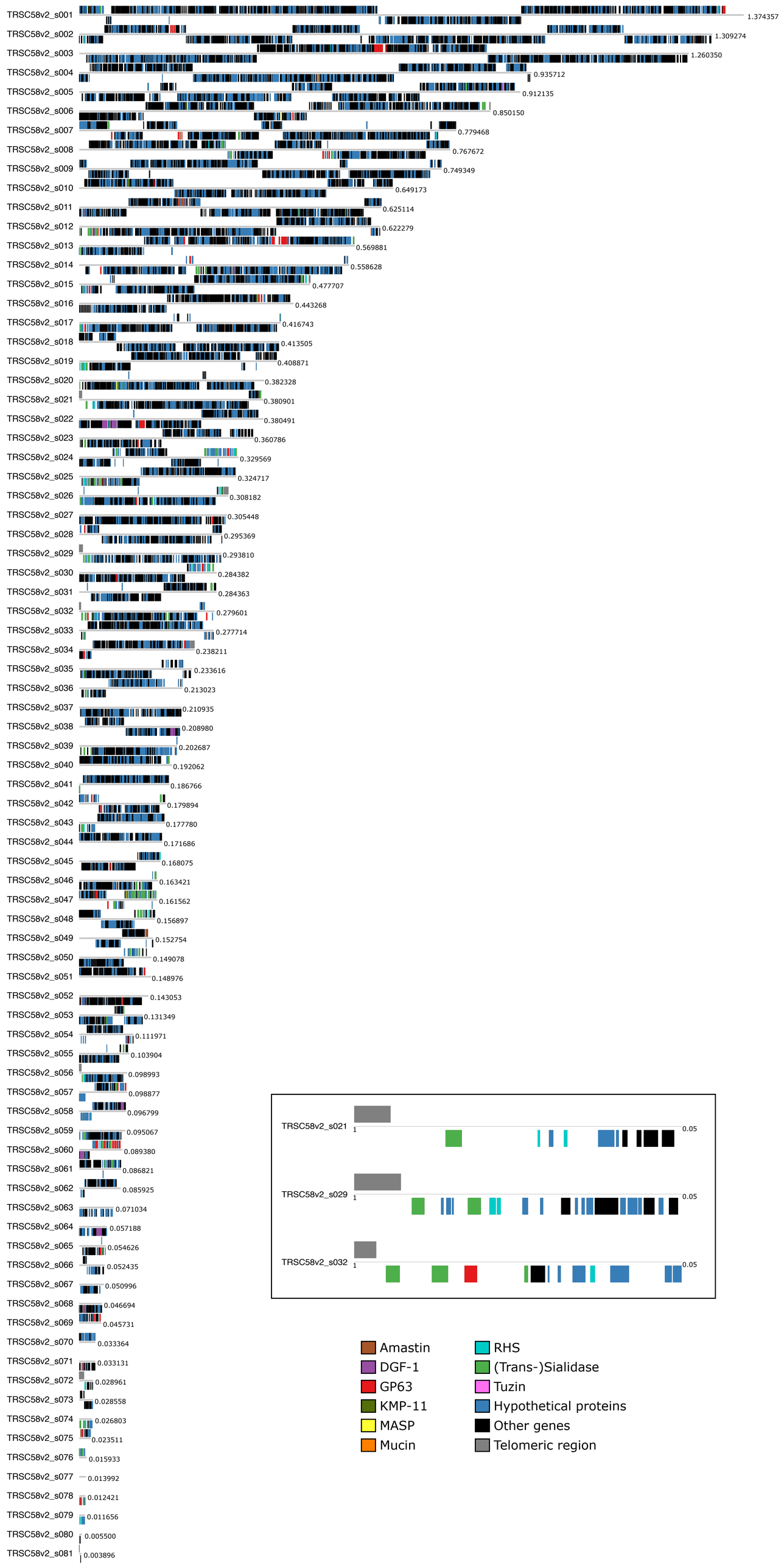
TRSC58v2_s001 1.374357
TRSC58v2_s002 1.309274
TRSC58v2_s003 1.260350
TRSC58v2_s004 0.935712
TRSC58v2_s005 0.912135
TRSC58v2_s006 0.850150
TRSC58v2_s007 0.779468
TRSC58v2_s008 0.767672
TRSC58v2_s009 0.749349
TRSC58v2_s010 0.649173
TRSC58v2_s011 0.625114
TRSC58v2_s012 0.622279
TRSC58v2_s013 0.569881
TRSC58v2_s014 0.558628
TRSC58v2_s015 0.477707
TRSC58v2_s016 0.443268
TRSC58v2_s017 0.416743
TRSC58v2_s018 0.413505
TRSC58v2_s019 0.408871
TRSC58v2_s020 0.382328
TRSC58v2_s021 0.380901
TRSC58v2_s022 0.380491
TRSC58v2_s023 0.360786
TRSC58v2_s024 0.329569
TRSC58v2_s025 0.324717
TRSC58v2_s026 0.308182
TRSC58v2_s027 0.305448
TRSC58v2_s028 0.295369
TRSC58v2_s029 0.293810
TRSC58v2_s030 0.284382
TRSC58v2_s031 0.284363
TRSC58v2_s032 0.279601
TRSC58v2_s033 0.277714
TRSC58v2_s034 0.238211
TRSC58v2_s035 0.233616
TRSC58v2_s036 0.213023
TRSC58v2_s037 0.210935
TRSC58v2_s038 0.208980
TRSC58v2_s039 0.202687
TRSC58v2_s040 0.192062
TRSC58v2_s041 0.186766
TRSC58v2_s042 0.179894
TRSC58v2_s043 0.177780
TRSC58v2_s044 0.171686
TRSC58v2_s045 0.168075
TRSC58v2_s046 0.163421
TRSC58v2_s047 0.161562
TRSC58v2_s048 0.156897
TRSC58v2_s049 0.152754
TRSC58v2_s050 0.149078
TRSC58v2_s051 0.148976
TRSC58v2_s052 0.143053
TRSC58v2_s053 0.131349
TRSC58v2_s054 0.111971
TRSC58v2_s055 0.103904
TRSC58v2_s056 0.098993
TRSC58v2_s057 0.098877
TRSC58v2_s058 0.096799
TRSC58v2_s059 0.095067
TRSC58v2_s060 0.089380
TRSC58v2_s061 0.086821
TRSC58v2_s062 0.085925
TRSC58v2_s063 0.071034
TRSC58v2_s064 0.057188
TRSC58v2_s065 0.054626
TRSC58v2_s066 0.052435
TRSC58v2_s067 0.050996
TRSC58v2_s068 0.046694
TRSC58v2_s069 0.045731
TRSC58v2_s070 0.033364
TRSC58v2_s071 0.033131
TRSC58v2_s072 0.028961
TRSC58v2_s073 0.028558
TRSC58v2_s074 0.026803
TRSC58v2_s075 0.023511
TRSC58v2_s076 0.015933
TRSC58v2_s077 0.013992
TRSC58v2_s078 0.012421
TRSC58v2_s079 0.011656
TRSC58v2_s080 0.005500
TRSC58v2_s081 0.003896
TRSC58v2_s021
1
0.05
TRSC58v2_s029
1
0.05
TRSC58v2_s032
1
0.05
Amastin
DGF-1
GP63
KMP-11
MASP
Mucin
RHS
(Trans-)Sialidase
Tuzin
Hypothetical proteins
Other genes
Telomeric region

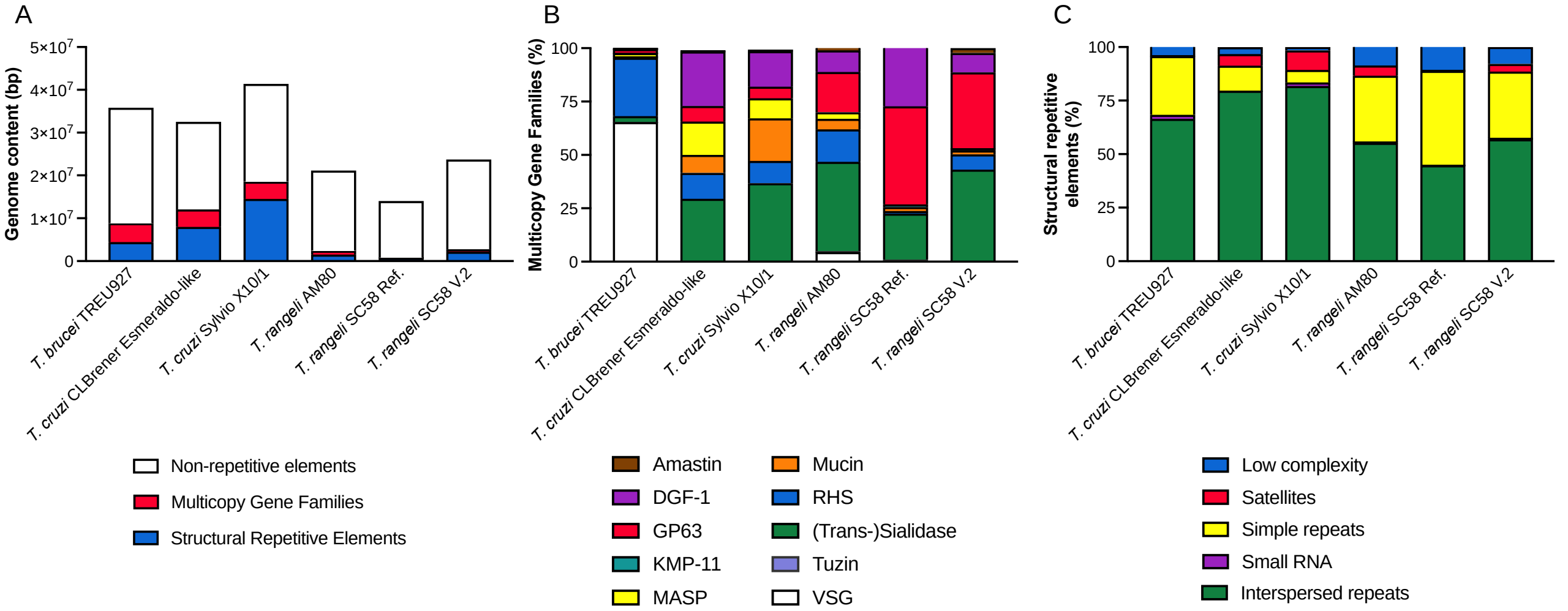
A
Genome content (bp)
5×10^7
4×10^7
3×10^7
2×10^7
1×10^7
0
T. brucei TREU927
T. cruzi CLBrener Esmeraldo-like
T. cruzi Sylvio X10/1
T. rangeli AM80
T. rangeli SC58 Ref.
T. rangeli SC58 V.2
B
Multicopy Gene Families (%)
100
75
50
25
0
C
Structural repetitive elements (%)
Non-repetitive elements
Multicopy Gene Families
Structural Repetitive Elements
Amastin
DGF-1
GP63
KMP-11
MASP
Mucin
RHS
(Trans-)Sialidase
Tuzin
VSG
Low complexity
Satellites
Simple repeats
Small RNA
Interspersed repeats

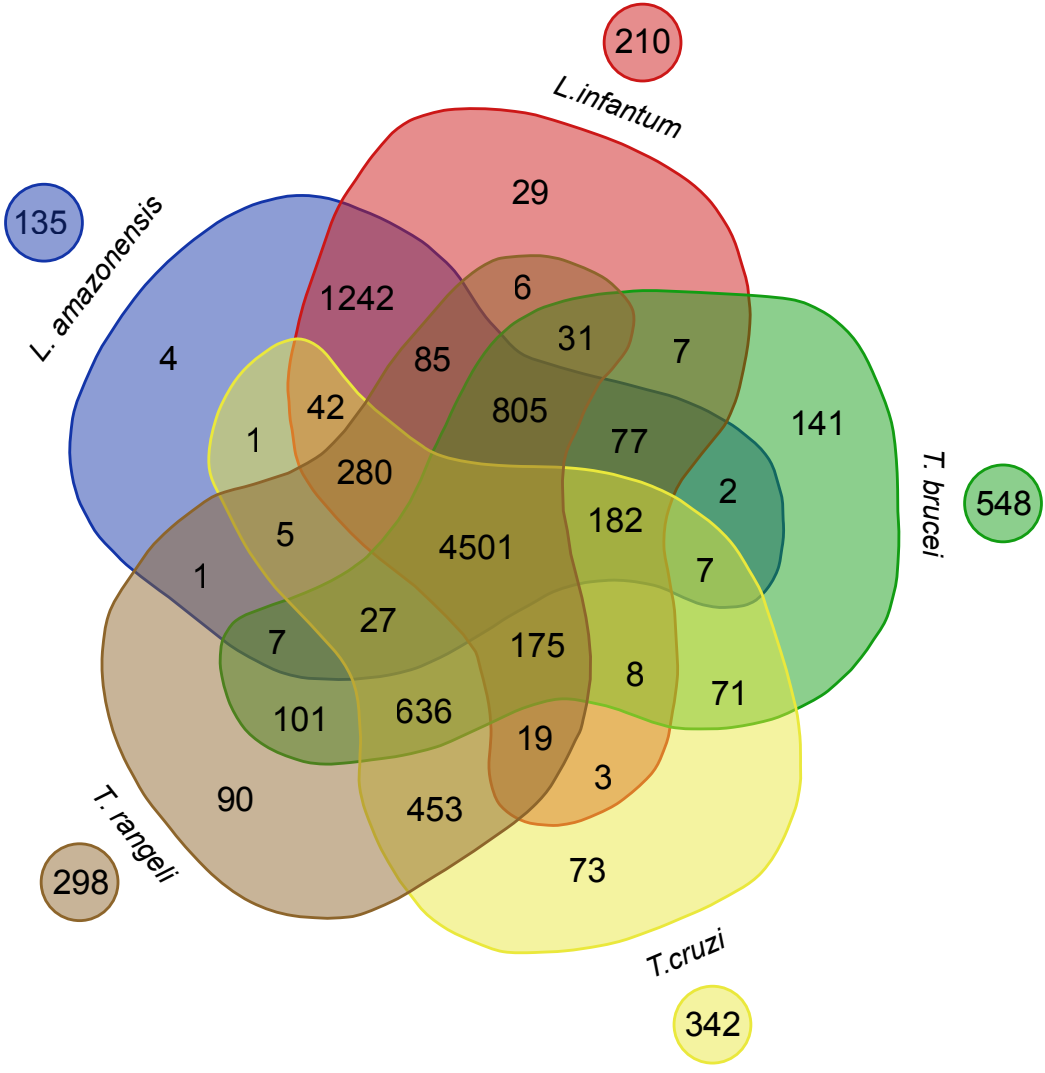
210
L.infantum
135
L. amazonensis
548
T. brucei
298
T. rangeli
342
T.cruzi
29
4
1242
6
85
31
7
42
805
141
1
77
280
2
5
182
4501
1
7
27
7
175
8
71
101
636
19
3
90
453
73

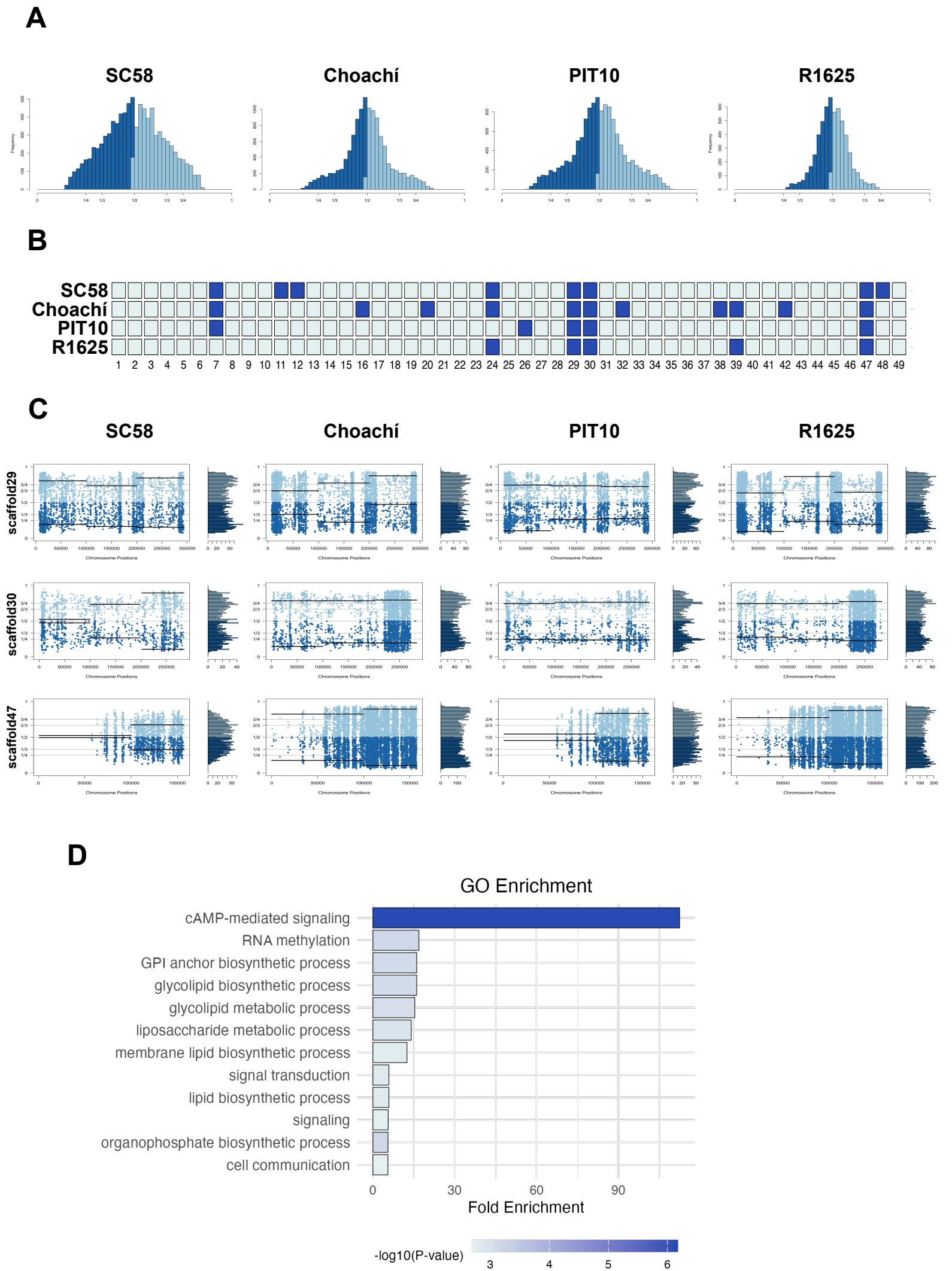
A
SC58
Choachí
PIT10
R1625
B
SC58
Choachí
PIT10
R1625
1 2 3 4 5 6 7 8 9 10 11 12 13 14 15 16 17 18 19 20 21 22 23 24 25 26 27 28 29 30 31 32 33 34 35 36 37 38 39 40 41 42 43 44 45 46 47 48 49
C
SC58
Choachí
PIT10
R1625
scaffold29
scaffold30
scaffold47
Chromosome Positions
D
GO Enrichment
cAMP-mediated signaling
RNA methylation
GPI anchor biosynthetic process
glycolipid biosynthetic process
glycolipid metabolic process
liposaccharide metabolic process
membrane lipid biosynthetic process
signal transduction
lipid biosynthetic process
signaling
organophosphate biosynthetic process
cell communication
0
30
60
90
Fold Enrichment
-log10(P-value)
3
4
5
6

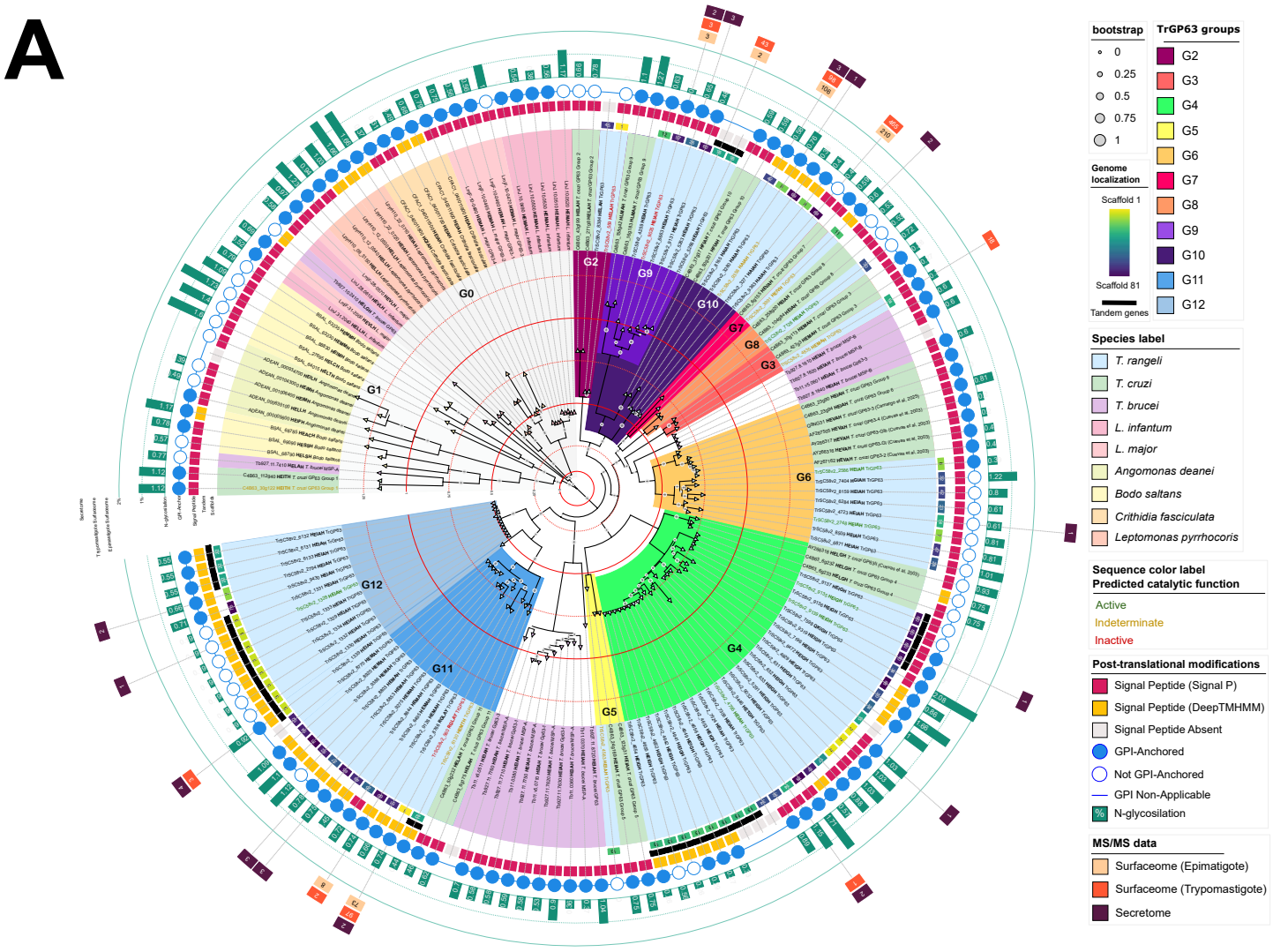
A
bootstrap
0
0.25
0.5
0.75
1
TrGP63 groups
G2
G3
G4
G5
G6
G7
G8
G9
G10
G11
G12
Genome localization
Scaffold 1
Scaffold 81
Tandem genes
Species label
T. rangeli
T. cruzi
T. brucei
L. infantum
L. major
Angomonas deanei
Bodo saltans
Crithidia fasciculata
Leptomonas pyrrhocoris
Sequence color label
Predicted catalytic function
Active
Indeterminate
Inactive
Post-translational modifications
Signal Peptide (Signal P)
Signal Peptide (DeepTMHMM)
Signal Peptide Absent
GPI-Anchored
Not GPI-Anchored
GPI Non-Applicable
N-glycosilation
MS/MS data
Surfaceome (Epimatigote)
Surfaceome (Trypomastigote)
Secretome
G0
G1
G2
G3
G4
G5
G6
G7
G8
G9
G10
G11
G12

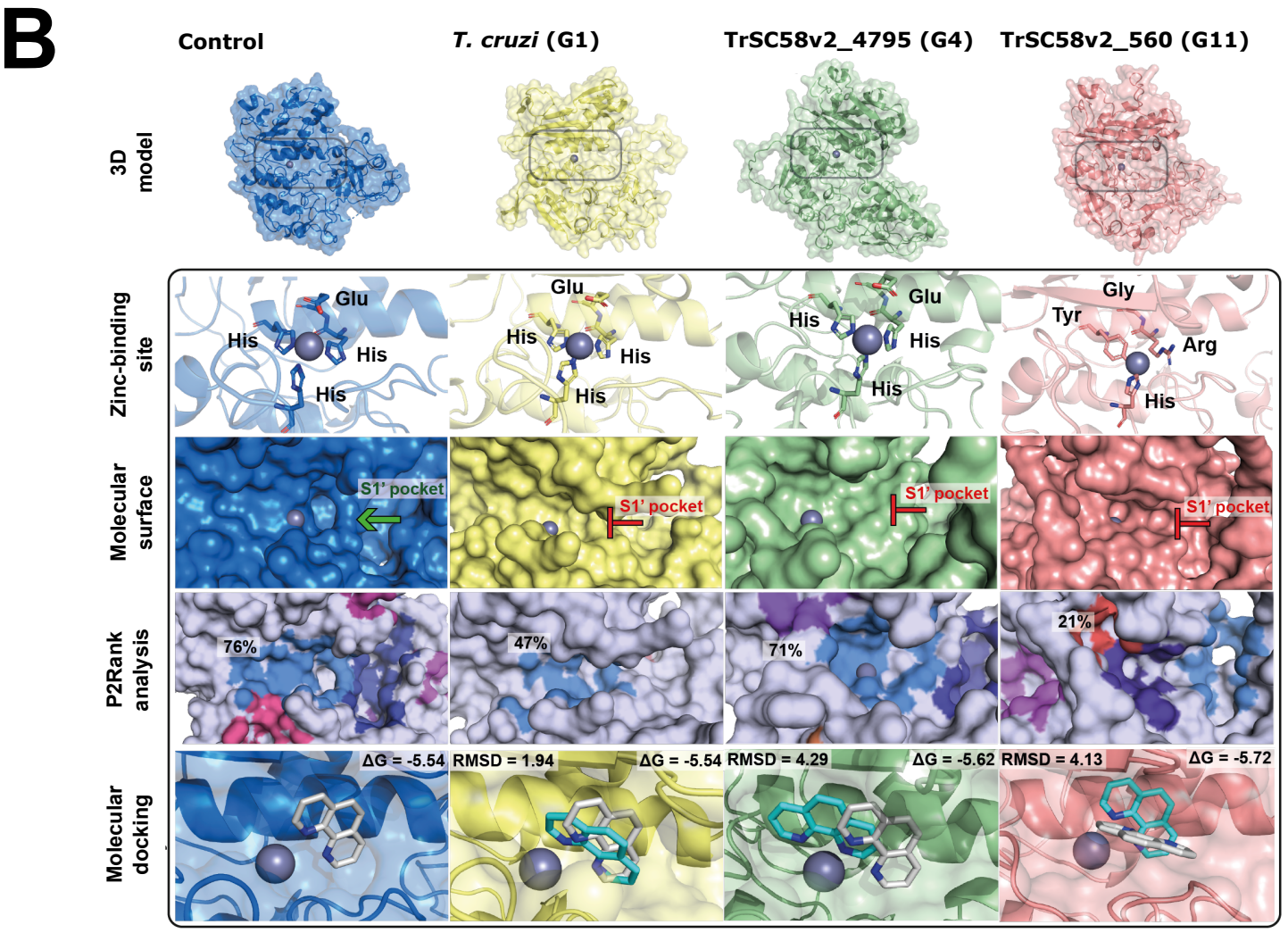
B
Control
T. cruzi (G1)
TrSC58v2_4795 (G4)
TrSC58v2_560 (G11)
3D model
Zinc-binding site
Molecular surface
P2Rank analysis
Molecular docking
Glu
His
His
His
Glu
His
His
His
Glu
His
His
His
Gly
Tyr
Arg
His
S1' pocket
S1' pocket
S1' pocket
S1' pocket
76%
47%
71%
21%
ΔG = -5.54
RMSD = 1.94
ΔG = -5.54
RMSD = 4.29
ΔG = -5.62
RMSD = 4.13
ΔG = -5.72

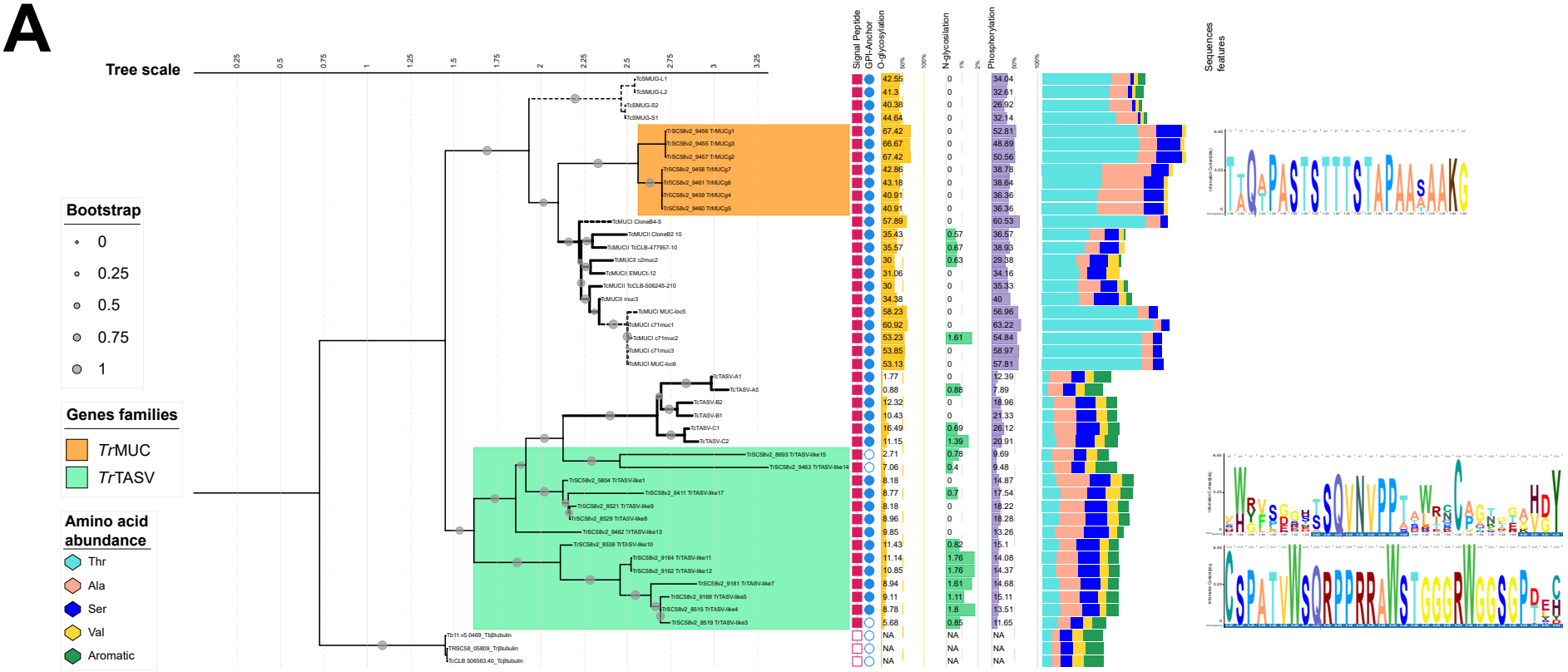
A
Tree scale
Bootstrap
0
0.25
0.5
0.75
1
Genes families
TrMUC
TrTASV
Amino acid abundance
Thr
Ala
Ser
Val
Aromatic
Signal Peptide
GPI-Anchor
O-glycosylation
N-glycosilation
Phosphorylation
Sequences features

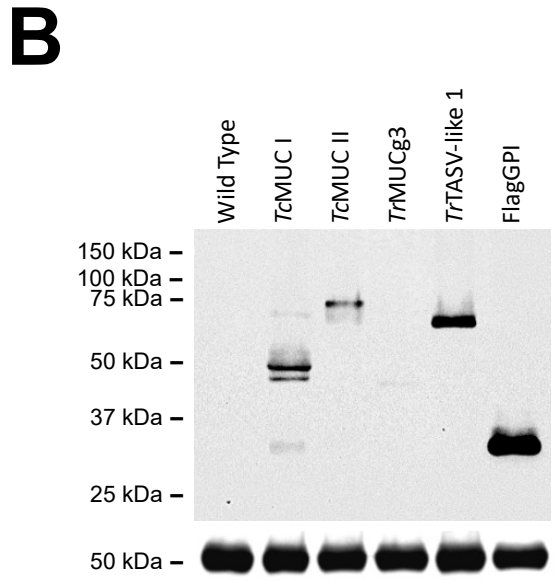
B
Wild Type
TcMUC I
TcMUC II
TrMUCg3
TrTASV-like 1
FlagGPI
150 kDa
100 kDa
75 kDa
50 kDa
37 kDa
25 kDa
50 kDa

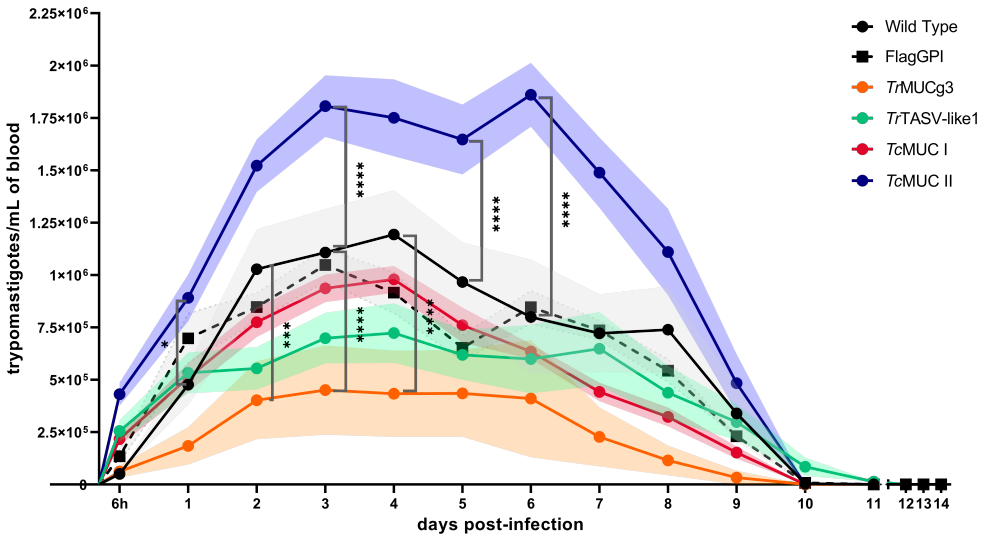
C
Wild Type
FlagGPI
TrMUCg3
TrTASV-like1
TcMUC I
TcMUC II
trypomastigotes/mL of blood
days post-infection
2.25×10⁶
2×10⁶
1.75×10⁶
1.5×10⁶
1.25×10⁶
1×10⁶
7.5×10⁵
5×10⁵
2.5×10⁵
0
6h
1
2
3
4
5
6
7
8
9
10
11
12
13
14